UCRL- 1278

UNIVERSITY OF CALIFORNIA — BERKELEY

TWO-WEEK LOAN COPY

This is a Library Circulating Copy which may be borrowed for two weeks. For a personal retention copy, call Tech. Info. Division, Ext. 5545

RADIATION LABORATORY

DISCLAIMER

This document was prepared as an account of work sponsored by the United States Government. While this document is believed to contain correct information, neither the United States Government nor any agency thereof, nor the Regents of the University of California, nor any of their employees, makes any warranty, express or implied, or assumes any legal responsibility for the accuracy, completeness, or usefulness of any information, apparatus, product, or process disclosed, or represents that its use would not infringe privately owned rights. Reference herein to any specific commercial product, process, or service by its trade name, trademark, manufacturer, or otherwise, does not necessarily constitute or imply its endorsement, recommendation, or favoring by the United States Government or any agency thereof, or the Regents of the University of California. The views and opinions of authors expressed herein do not necessarily state or reflect those of the United States Government or any agency thereof or the Regents of the University of California.

UCRL-1278
Unclassified-Physics Distribution
Copy 2

UNIVERSITY OF CALIFORNIA

Radiation Laboratory

Contract No. W-7405-eng-48

PRODUCTION OF π^+-MESONS BY 340 MEV PROTONS ON PROTONS AT 0° TO THE BEAM

W. F. Cartwright

(Thesis)

April 16, 1951

Berkeley, California

OUTLINE

I. Introduction

II. General Method

III. Details of the Method

- A. Target
- B. Magnetic Field
- C. Channel
- D. Meson Background
- E. Geometry
- F. Detector
- G. Detection Efficiency
- H. Calculation of Cross-Section
- I. Corrections to Cross-Section
  - 1. Decay in Flight
  - 2. Nuclear Absorption and Scattering
  - 3. Thick Target

IV. Results

V. Discussion

VI Meson Mass Determination

VII. Acknowledgments

VIII. Appendices

Appendix 1. Solid Angle Calculation

- A. In a Uniform Magnetic Field
- B. Corrections

Appendix 2. Dynamics

Appendix 3. Resolution

Appendix 4. Thick Target Compensation

IX. References

X. Figure Captions
Figures 1 - 19

PRODUCTION OF π^+-MESONS BY 340 MEV PROTONS ON PROTONS AT 0° TO THE BEAM

W. F. Cartwright
April 16, 1951

I. INTRODUCTION

The meson production processes most simply analyzed theoretically are those in photon-nucleon and nucleon-nucleon interactions. The first investigations, at the 184-inch synchro-cyclotron, of the cross-sections for the production of mesons by protons on various complex nuclei[1,2] indicated that the cross-section for production of mesons from the proton-proton interaction would be sufficiently high to be measurable by the techniques then developed. Consequently two groups of workers undertook the measurement of the energy spectrum of π^+-mesons produced by protons on protons. The group headed by Professors Richman and Wilcox, using a magnetic field to separate mesons from background particles, measured the production spectrum at 0°[3] and later at 60°[4] to the proton beam. In each case the hydrogen spectrum was found by a polyethylene - carbon difference method. Peterson, Iloff, and Sherman measured the spectra at 30°[5] and 18°[6] by use of a liquid hydrogen target.

In the early work, an intense peak was discovered in the spectrum at high meson energies. The successful attempt to explain this theoretically led to the development of a phenomenological theory of meson production by Watson and Brueckner[7,8]. This theoretical study indicated that a more careful experimental investigation of the spectrum of mesons produced by protons on protons was warranted in order to determine critical values in the phenomenological explanation of the production process.

Consequently the method of the Richman - Wilcox group was used to measure more accurately the differential cross-section as a function of energy in the forward direction. Presented here are the results of this detailed investigation.

In addition to the theoretical interest which attaches to the cross-section measurements of this experiment, the high peak in the spectrum provides a means of determining the π^+-meson mass. This determination is discussed in Section VI.

II. GENERAL METHOD

The method used to measure the $p + p \rightarrow \pi^+$ cross-section is essentially a modification of the method developed by Richman and Wilcox in their measurement of the production of mesons at 90° by protons interacting with carbon[1]. In that scheme the mesons produced by protons in the external beam of the synchro-cyclotron were slowed down by ionization in some absorbing medium and the population of stopped mesons was sampled by a nuclear emulsion inserted in the absorber. The endings of the meson tracks in the emulsion were examined under high magnification and the mesons identified as positive if they decayed into μ mesons or as negative if they initiated a nuclear star. By relating the number of stopped mesons, the emulsion thickness, the stopping power of the absorber, and the distance of the emulsion from the carbon target, cross-sections for the production of positive and negative mesons by 340 Mev protons on carbon were deduced. Since the distance the meson penetrates into the absorber is related in a known manner to its energy, the cross-sections were found as a function of energy by inserting emulsions at various depths in the absorber. This work was all done at 90° to the proton beam.

The number of background particles produced in the forward direction makes cross-section measurements at forward angles very difficult with the simple scheme outlined above. At zero degrees, the background due to the proton beam itself would make the measurement impossible.

The following modification has been developed in order to measure meson production cross-sections at any angle to the beam for any given meson energy.

(Fig. 1 shows a schematic diagram of a typical arrangement used in the experiment.) The target and absorber-detector are placed in a magnetic field so that mesons produced in the target circle away from the protons in the beam. Because of their high energy and large mass, the protons have trajectories of very large radius compared to those of the mesons. Protons inelastically scattered from the target will follow the same trajectories as the mesons only if they possess the same momentum. It can be shown from the range-energy relations that a meson has a range which is about 140 times as large as the range of a proton of the same momentum. Thus, in the region of the absorber in which the mesons are stopped, the background due to heavier charged particles following the same trajectories as the mesons is eliminated.

Background from particles which might follow different paths than the mesons in travelling from the target to the emulsion is reduced by means of brass shielding. The mesons of interest travel down a channel cut into this shielding.

The experiment was done under "poor geometry" conditions. The mesons, in penetrating into the absorber containing the emulsion, experience small angle scattering. Therefore, in order to have as many mesons scatter into the emulsion as scatter out, the meson beam impinging on the absorber must be large in transverse dimensions compared to the root mean square displacement that the mesons undergo in reaching the end of their range. Thus, the exit of the meson channel has specified minimum dimensions. In addition, the channel is constructed so that mesons of the energy interval under consideration can leave any part of the target and reach any part of the channel exit. Poor geometry is thus obtained for this whole energy interval of mesons being detected.

The mesons sampled by this arrangement are produced with a small spread of angles and in a small energy interval. In order to determine the entire

meson spectrum at any particular angle of production, several experimental runs are made, each sampling mesons in a different momentum range.

The complete angular distribution can be obtained by merely changing the direction with which the proton beam strikes the target. This paper explains in detail the measurements made at 0° to the beam.

All the experiments were done in the external beam of the synchro-cyclotron. This made it possible to determine the cross-sections on an absolute scale, since the total proton charge could be accurately measured by a calibrated ion chamber.

III. DETAILS OF THE METHOD

A. Target

Pure hydrogen, liquid or gaseous, suggests itself for the target to be used in a direct measurement of the cross-section. There are, however, disadvantages in using such a target, most of them mechanical. The principal objection is the difficulty of measuring the production at 0°: the heavy container of the dense liquid or gaseous hydrogen must be placed in a magnetic field if the mesons produced by the protons passing through the container walls are to be distinguished from those produced by the protons on the hydrogen. In addition, the container walls impose the necessity of applying corrections to the observed energies of both mesons and protons.

In the hope that the hydrogen cross-section was perhaps fairly large, the meson production from both polyethylene, $(CH_2)_n$, and carbon was measured. As will be shown later, the high cross-section of hydrogen does indeed make it possible to obtain the proton-proton meson production spectrum with good accuracy by subtracting the carbon spectrum from the CH_2 spectrum.

A calculation of the meson production cross-section requires an exact knowledge of the position at which the mesons are produced. Such information

is necessary in order accurately to determine the solid angle which the detector subtends at the point of production, the number of mesons which decay in flight, and the energy loss that the mesons and protons suffer by ionization in passing through the target.

This requirement for a compact target was satisfied by the use of polyethylene and carbon. The density of hydrogen in polyethylene is sufficiently high and the external proton beam of the cyclotron intense enough to permit the use of 1/4 inch to 1/2 inch thick targets. The effective area of the target was that of the external beam of the cyclotron. A one inch collimator in the concrete shielding of the machine produced, therefore, a cylindrical target of 1 inch diameter.

B. Magnetic Field

The magnetic field used in the original investigation to separate the meson trajectories from the proton beam was produced by a magnet whose maximum field was about 13,000 gauss. The pole faces were rectangular in shape, 12 inches by 30 inches, and were separated by a gap of 2.74 inches.

A pair spectrometer magnet, constructed for use at the synchro-cyclotron, became available soon after the initial measurement of the spectrum was made. The field of this magnet, with a 3.5 inch gap, had a maximum value of about 14,300 gauss; this field was effective over an area sufficiently large to turn a 70 Mev meson trajectory through about 90°. (See Fig. 1.) Because of the larger gap, the number of heavy particles scattered by the pole faces was decreased by using this magnet. In addition, the larger field made it possible to bend the trajectories further away from the beam. These two effects produced a great improvement in the meson to background ratio. The detailed investigation at the peak of the meson spectrum was made employing the pair spectrometer magnet.

The magnetic field was calibrated by means of a nuclear induction measurement, accurate to at least 0.5 percent. The variation in time of the field during any particular run never exceeded 1 percent.

C. Channel

The purpose of the brass shielding (see Fig. 1) is to discriminate against protons and background particles produced in the target. Without such shielding these particles could, by leaving the target at angles other than 0°, reach the detector by other trajectories than those followed by the mesons of interest.

The width of the meson channel in the brass shielding is required to be large compared to the mean lateral displacement that a meson undergoes by multiple scattering in the absorber holding the nuclear emulsions. At the same time, the channel must allow mesons in the desired energy range to reach all points of the detector-absorber face from each part of the target. The rms lateral displacement was calculated by means of the approximate relation[9] $y_{rms} = 0.03 \sqrt{Z} R$. The channel exit width was then designed to be equal to about $2.5\ y_{rms}$. (The channel exit height was always much larger than $2.5\ y_{rms}$.)

It is desirable to examine as much of the spectrum as possible in each cyclotron run. However, the acceptance of a large energy interval requires a wide channel, and this decreases the efficacy of the brass shielding. Thus a compromise was made between the conflicting requirements of maximum information per run and minimum background. At the high energy region of the spectrum it was found feasible to use a channel accepting a 20 Mev interval. Therefore, it was possible to cover the region of the peak in one run. A total of three runs were made, each with a different channel, in order to complete the investigation of the spectrum.

D. Meson Background

The mesons produced by those proton which were scattered from the target

into the pole faces of the magnet formed the meson background. An approximate calculation of the number produced in that region of the pole faces from which mesons could reach the channel exit led to an extreme upper limit for the background of 7 percent.

Only an indication of the background is available experimentally, since a removal of the target would eliminate the scatterer. Instead of such a removal, a run was made with the magnetic field removed. No mesons from the target could then reach the plates. No mesons were found in the plates, and the volume of emulsion scanned led to an upper limit of less than 10 percent background.

A further indication of the low background is the absence of negative mesons in the emulsions scanned. Although the magnetic field and channel select only positive mesons produced in the target in the forward direction, they also accept from a large area of the pole faces, negative mesons produced by scattered protons. The total number of mesons counted in the experiment was 1121. The complete absence of any π^--mesons indicates a negligible meson background, and consequently no background correction was made.

E. Geometry

In a uniform magnetic field, H, the motion of a meson in a plane perpendicular to the lines of force will be along the arc of a circle whose radius of curvature is $\rho = \frac{pc}{eH}$, where p is the meson momentum. The solid angle subtended at the target by unit area perpendicular to a pencil of meson trajectories, after the tangent to the mean trajectory has turned through an angle φ, is given by

$$\frac{d\Omega}{dA} = \frac{1}{\rho^2 \varphi \sin \varphi} \text{ ster.}/\text{cm}^2, \qquad (1)$$

if the trajectories are approximately perpendicular to the lines of force. (See Appendix 1.)

It is considerably easier to calculate the solid angle subtended at the target by unit area at the photographic emulsion, if the emulsion is placed in the gap where the field is uniform. Outside the gap corrections have to be made to Eq. (1) because of the change in the radius of curvature and the forces due to the fringing field. It was found, however, that a small increase in the distance travelled by the mesons decreased the background tracks on the emulsions appreciably. For this reason, the emulsions were placed not in the gap, but immediately outside where the corrections can still be made with good accuracy. These corrections are discussed in Appendix 1. With this arrangement, the solid angle per unit area at the emulsion is given by

$$\frac{d\Omega}{dA} = \frac{1}{\rho^2 \left(\varphi + \frac{x}{\rho}\right)(\sin\varphi)\left[1 + \frac{x}{\rho}\cot\varphi\right]} \frac{\text{ster.}}{\text{cm}^2} \qquad (2)$$

where φ is the angle through which the tangent to the trajectory turns up to the pole face edge, and x is the distance from the edge to the emulsion. It is shown in Appendix 1 that this equation is not subject to more than 1 percent error.

F. Detector

The nuclear emulsions used were Ilford C-2 and C-3, which are sensitive enough to record the μ meson produced in the decay of the π^+-meson at the end of its range. For ease of detection the plates were oriented nearly parallel to the meson beam so that the mesons travelled approximately in the plane of the emulsion before stopping.

The absorber in which the emulsions were embedded was aluminum. For high energies, near the peak in the meson spectrum, a copper slab was placed in front of the aluminum absorber holding the emulsion (see Fig. 2). With this arrangement, the mesons lost most of their energy by travelling a short distance in the copper, and the energy spectrum was spread out along the nuclear

plate because of the low stopping power of the aluminum. The range-energy curves of Aron, Hoffman, and Williams[10], as corrected by the recent work of Mather and Segre[11], were used to convert the meson range to energy. These latest corrected curves are accurate to about 0.5 percent in energy.

The absorber face was cut so that the mesons entered normally. With this arrangement, the variation in depth of penetration with angle of incidence is a minimum. With a 1 inch diameter target, and the maximum channel width used, this angle varied between -3° and $+3^{\circ}$, depending on the energy of the meson and its points of origin and decay. This produced an uncertainty in depth of penetration of less than 0.2 percent.

G. Detection Efficiency

The number of mesons impinging on the absorber can be deduced from the number stopping in the plate by the following argument. We assume, for the moment, no scattering.

Mesons of energy E in the beam will stop in the absorber at a range R_o given by the range-energy relation. However, those mesons whose trajectories lie between M_1 and M_2 (see Fig. 3) will stop in the emulsion, while mesons whose trajectories lie outside these two will stop only in the aluminum absorber. It is easy to show that the distance a between these two trajectories is given by

$$a = d \sec \alpha \frac{R_{ab}}{R_{em}} \qquad (3)$$

where R_{em} and R_{ab} are the residual ranges of a meson of energy E_{res}, the residual energy, in emulsion and absorbing material respectively. For the angle α used, 15°, and the thickness d of emulsion, about 200 microns, E_{res} is about 7 Mev. For aluminum and emulsion the ratio R_{ab}/R_{em} is 1.20. The number of mesons of energy E in ΔE that stop in a strip of emulsion of length ℓ (perpen-

dicular to the paper in Fig. 3) is then equal to $N_o(E)\Delta E$ times the area a x ℓ, where $N_o(E)\Delta E$ is the number of mesons of initial energy E in ΔE per square cm in the beam coming into the emulsion.

The spread in meson energy, ΔE, in the beam, corresponding to a distance Δz along the plate is given by

$$\Delta E = \frac{dE}{dx} \Delta Z \cos \alpha \tag{4}$$

where dE/dx is the rate of energy loss in the absorber at the initial energy of the mesons in the beam. Thus, the number of mesons that stop in the area $\Delta Z \times \ell$ on the plate is given by

$$n = N_o(E)\frac{dE}{dx} \cos \alpha \; a \, \ell \Delta Z. \tag{5}$$

So,

$$N_o(E) = \frac{n}{\frac{dE}{dx} \frac{R_{ab}}{R_{em}} \ell d \; \Delta Z} = \frac{\rho_n}{\frac{dE}{dx} \frac{R_{ab}}{R_{em}}}. \tag{6}$$

The number of mesons per cm^2 per Mev in the beam is thus given in terms of ρ_n, the number of mesons found per unit volume of the emulsion. The thickness, d, of the emulsion was measured by a method devised by H. A. Wilcox[12].

The trajectories of the mesons are in fact not straight, as was assumed in the above calculation, and it might be expected that the small angle scattering would change the relation given in Eq. (6) appreciably. It is not difficult to prove, however, that the detection efficiency of the emulsion is independent of the angles that the meson trajectories make with either the absorber face or the plane of the emulsion. Consequently, Eq. (6) always gives the relationship between the flux of mesons of initial energy E impinging on a certain region of the emulsion and the density of stopped mesons in that region.

If a narrow beam of mesons is incident on the absorber face, however,

the flux would be decreased by scattering as the mesons traverse the absorber. It was for this reason that the meson channel was made wide in order to ensure poor geometry. For this case, the flux remains unaffected by scattering as the meson beam penetrates the absorber. Thus Eq. (6), although calculated assuming no scattering, is in general true.

H. Calculation of Cross-Section

In order to measure the cross-section for production on an absolute scale, the number of bombarding protons, the number of target nuclei per cm^2, and the number of mesons produced in the angular and energy intervals of interest must all be measured. By integrating the external proton beam during the bombardment using a calibrated ionization chamber, the number of bombarding protons was obtained to an accuracy estimated to be better than 5 percent. The densities of the targets were easily determined from their weights and their simple dimensions.

To find the number of mesons produced per steradian per Mev, one needs the solid angle subtended at the target by unit area at the emulsion, and the emulsion detection efficiency. As has been shown, these can both be calculated in a straightforward manner.

The number of mesons of energy E per Mev per cm^2 in the beam is given by

$$N_o(E) = \eta \frac{qtA_o}{A} \frac{d\sigma}{dEd\Omega} \frac{d\Omega}{dA} \tag{7}$$

where η is the number of protons that passed through the target, q is the density of the target material, A_o is Avagadro's number, A is the molecular weight of carbon or CH_2, t is the target thickness, $\frac{d\sigma}{dEd\Omega}$ is the differential cross-section for production of mesons by protons on a carbon nucleus (or a CH_2 group) per unit solid angle per Mev, and $\frac{d\Omega}{dA}$ is the solid angle per unit area at the emulsion.

Using Eqs. (6) and (7), the differential cross-section is therefore found to be

$$\frac{d\sigma}{dE\,d\Omega} = \frac{\rho_n}{\frac{dE}{dx}\,\frac{R_{ab}}{R_{em}}\,\eta\,qt\,\frac{A_o}{A}\,\frac{d\Omega}{dA}}\ \frac{\overline{cm}^2}{\text{Mev-steradian}}. \tag{8}$$

I. Corrections to Cross-Section

Three corrections have to be made to Eq. (8). Two of these take into account the decrease in the number of mesons that reach the detector because of 1) their decay in flight and 2) their absorption and large angle scattering by nuclei in the copper and aluminum absorbers. The third correction arises from the use of a "thick" production target.

1. Decay in Flight

The lifetime of the π^+-meson against decay into a μ-meson has been measured as 2.6×10^{-8} sec.[13] In the meson's frame of reference an interval of time $d\tau$ elapses while the meson travels a distance dr in the laboratory system, where

$$d\tau = \frac{m_\pi c^2\,dr}{p\,c^2}. \tag{9}$$

For that part of the meson path that is in air, the meson energy remains very nearly constant, and the time taken to travel the distance r from the target to the absorber face is just

$$\tau_{air} = \frac{r m_\pi c^2}{p\,c^2}. \tag{10}$$

Since this part of the travel is in a uniform magnetic field,

$$r = \rho\varphi \tag{11}$$

and

$$p = \frac{H\rho e}{c}, \tag{12}$$

where Φ is the angle through which the meson's velocity vector turns. Thus,

$$\tau_{air} = \frac{\varphi}{Hec} m_\pi c^2 . \tag{13}$$

For mesons, this becomes

$$\tau_{air} = 15 \times 10^{-6} \frac{\varphi}{H} \text{sec.} \tag{14}$$

An analytical expression for the time required for the meson to stop in the absorber can be obtained by making use of the approximate range-energy relation[14]

$$E_\pi = K R^{.58} . \tag{15}$$

With this relation, it can be shown that

$$\tau_{abs.} = 8.0 \times 10^{-11} \sqrt{\frac{m_\pi c^2}{2E_o}} R_o^{.71} \text{ sec.}, \tag{16}$$

where R_o is the range in cm of the meson of initial energy E_o in the absorber.

Since the mean life is 2.6×10^{-8} sec, the total correction factor due to decay in flight is

$$\frac{\sigma_{corr.}}{\sigma_{un.}} = e^{\frac{10^8}{2.6}\left[15 \times 10^{-6} \frac{\varphi}{H} + 8.0\sqrt{\frac{m_\pi c^2}{2E_o}} R_o^{.71} \times 10^{-11}\right]} \tag{17}$$

This correction factor is listed in Column 3 in Table I (see Section IV), as a function of the meson energy.

2. Nuclear Absorption and Scattering

An experimental measurement of the nuclear absorption and large angle scattering cross-section for mesons in aluminum and copper has not to date been made. Present indications[15], however, give nuclear area as the order of magnitude for the combined cross-section for these two effects. To deduce the decrease in flux, therefore, we have assumed an attenuation cross-section of πr_o^2, where $r_o = 1.39 A^{1/3} \times 10^{-13}$ cm. A combination of copper and aluminum absorbers was

used in this experiment. From the above, the attenuation cross-sections are $\sigma(Al) = 5.5 \times 10^{-25}$ cm^2 and $\sigma(Cu) = 9.6 \times 10^{-25}$ cm^2.

Without the absorber, the flux per Mev is $N_o(E)$ at the emulsion. Insertion of a thickness t_{al} of aluminum and t_{cu} of copper reduces this to

$$N_o' = N_o\, e^{-A_o\left[\left(\frac{\sigma qt}{A}\right)_{cu} + \left(\frac{\sigma qt}{A}\right)_{Al}\right]} \quad ; \tag{18}$$

where q is the density, A_o is Avagadro's number, and A is the atomic weight The magnitude of this correction, as a function of the energy, is given in Column 4 in Table I (see Section IV). This correction, unfortunately, is not a small one. At the maximum meson energy it is about 25 percent. Therefore, in Table I(C), where the corrected values for $\frac{d\sigma}{dE d\Omega}$ are given, the values before the nuclear attenuation correction has been made are also tabulated.

3. Thick Target

By means of the emulsions, the number of mesons emerging from the target in an energy interval ΔE were measured. The mesons emerging in ΔE were, however, produced in the target in an energy interval δE where, because of the non-linear range-energy relation $\delta E < \Delta E$.

The relation between ΔE and $\overline{\delta E}$, the average energy interval at production, is found here. It is clear from Fig. 4, in which the target of thickness t is followed by a sea of the same material, that

$$\delta E = \left.\frac{dE}{dx}\right|_x (x_2 - x_1) \text{ and } \Delta E = \left.\frac{dE}{dx}\right|_t (x_2' - x_1'). \tag{19}$$

Also, $x_2 - x_1 = x_2' - x_1'$. So,

$$\delta E = \Delta E \left[\left.\frac{dE}{dx}\right|_x \Big/ \left.\frac{dE}{dx}\right|_t \right]. \tag{20}$$

The average δE corresponding to a given ΔE can be found if one assumes that the production spectrum is flat over the energy spread represented by the target. Then

$$\overline{\delta E} = \frac{\int_0^t (\delta E)\,dx}{t} = \frac{\Delta E}{t} \frac{1}{\left.\frac{dE}{dx}\right|_t} \int_0^t \left.\frac{dE}{dx}\right|_x dx \,. \tag{21}$$

Now, using Eq. (15), one obtains

$$\frac{dE}{dx} = .58K\, R^{-.42} \,. \tag{22}$$

So,

$$\left.\frac{dE}{dx}\right|_t = \frac{.58K}{R_o^{.42}} \quad \text{and} \quad \left.\frac{dE}{dx}\right|_x = \frac{.58K}{(R_o + x)^{.42}} \,. \tag{23}$$

Therefore,

$$\overline{\delta E} = \frac{\Delta E}{t} \int_0^t \frac{dx}{\left(1 + \frac{x}{R_o}\right)^{.42}} = \frac{\Delta E}{t} \frac{R_o}{.58} \left[\left(1 + \frac{t}{R_o}\right)^{.58} - 1 \right] . \tag{24}$$

Thus, since $\frac{d\sigma}{dE d\Omega}$ is inversely proportional to the energy interval, in order to find the true production cross-section one must multiply the right-hand side of Eq. (8) by

$$\frac{0.58\ t/R_o}{\left[\left(1 + \frac{t}{R_o}\right)^{.58} - 1\right]} \,. \tag{25}$$

For small values of t/R_o this becomes

$$\frac{\sigma_{corr.}}{\sigma_{un.}} = \frac{1}{1 - .21\ t/R_o} \,. \tag{26}$$

For the thin target used in the investigation of the peak, this correction is of the order of a few percent. At the lower energy points it becomes more

important. Its magnitude for each of the experimental points of the spectrum is given in Column 5 in Table I.

IV. RESULTS

This section presents the experimental results.

In Table I are listed the cross-sections for the production of π^+-mesons by 340 Mev protons on a CH_2 group (Table I(A)), a carbon nucleus (Table I(B)), and a free proton (Table I(C)). The date in Table I(C) is obtained by subtracting I(B) from I(A).

Column 1 gives the energy of production of the mesons, as deduced from their range. For example, the mesons at the peak of the CH_2 spectrum passed through, successively, 1/4 inch of CH_2 target, 56 cm of air, 1.36 cm of copper, and finally 3.10 cm of aluminum. Mesons with this range, having undergone no scattering would have started with 70.0 Mev, the energy assigned the experimental peak shown in Fig. 5. (Those mesons originating in the center of the 1/4 inch CH_2 target did not, of course, pass through the entire thickness of the target. However, it is shown in Appendix IV that peak energy mesons which are produced at the front of the target emerge from it with the same energy as those produced at the back by the protons which have also been degraded.)

Column 2 gives the cross-sections as calculated by Eq. (8). Columns 3, 4, and 5 give the correction factors due to decay in flight, nuclear absorption and scattering, and the thick target.

In Column 6 are given the final corrected cross-sections, and Column 7 gives the statistical probable errors. The absolute value of these cross-sections is assigned a probable error of ± 15 percent because of the uncertainties in the scanning efficiency of the observer, in the integration equipment, and in the stopping power of the emulsion.

In Column 8 are given the cross-sections for production from hydrogen, uncorrected for nuclear absorption.

As will be seen, by consulting Table I, the CH_2 peak was examined in detail, but only one point in this energy region was measured for carbon. This seems justified since the CH_2 spectrum is so intensely peaked that the exact details of the slowly changing carbon spectrum need not be known in order to get a good subtraction. However, also shown in Table I(B) are results on the production from carbon recently obtained by Merritt and Schulz[16], normalized so that their 74 Mev point agrees with the 70 Mev point from this experiment. Since the spectrum is apparently quite flat in the vicinity of the hydrogen peak, the value of 12.3×10^{-30} cm^2 Mev^{-1} $ster^{-1}$ was used for the carbon differential cross-section in the interval from 60 to 75 Mev.

Fig. 5 is a graph of the differential cross-section for the production of π^+-mesons by protons on protons as a function of the meson energy.

The integral of the hydrogen spectrum over the entire energy scale gives $\frac{d\sigma}{d\Omega} = 2.0 \pm 0.4$ cm^2 $ster^{-1}$.

The integral over the hydrogen peak alone, from 65.5 Mev to 76.0 Mev, which is shown in the next section to be a result of deuteron formation, gives $\frac{d\sigma}{d\Omega} = 1.3 \pm 0.3$ cm^2 $ster^{-1}$.

TABLE I

Differential Cross-Sections for the Production of π^+ Mesons by 340 Mev protons on CH_2 (Table IA); Carbon (Table IB); and Hydrogen (Table IC).

	Meson Energy (Mev)	$\frac{d\sigma}{d\Omega dE} 10^{30}$ $cm^2\ ster^{-1}\ Mev^{-1}$ (Eq.8)	Decay in Flight Correction Factor	Nuclear Absorption Correction Factor	Thick Target Correction Factor	$d\sigma_{corr}$ Corrected Differential Cross-Section $cm^2\ Mev^{-1}\ ster^{-1}$	Statistical Probable Error	$\frac{d\sigma}{d\Omega dE}$ Uncorrected for Nuclear Absorption
Table IA	17.5	3.0	1.13	1.02	1.11	3.8×10^{-30}	$\pm 0.6 \times 10^{-30}$	
$p + CH_2 \rightarrow \pi^+$	34.0	5.3	1.09	1.06	1.11	6.8	0.7	
	60.9	13.3	1.08	1.18	1.01	17.1	1.0	
	63.8	11.8	1.08	1.20	1.01	15.4	1.5	
	65.7	13.8	1.08	1.21	1.01	18.2	2.0	
	67.2	22.8	1.08	1.22	1.01	30.4	2.1	
	68.8	45.4	1.08	1.23	1.01	60.9	2.5	
	70.7	50.5	1.07	1.24	1.01	67.6	2.7	
	72.3	18.7	1.07	1.25	1.01	25.3	2.2	
	73.7	11.2	1.07	1.26	1.01	15.3	1.9	
	75.6	10.9	1.07	1.28	1.01	15.1	2.0	

Table I (con't.)

	Meson Energy	$\frac{d\sigma}{d\Omega dE} 10^{30}$ (Eq. 8)	Decay in Flight	Nuclear Absorption	Thick Target	$d\sigma_{corr}$ Corrected Differential Cross-Section $cm^2\ Mev^{-1}\ ster^{-1}$	Statistical Probable Error	$d\sigma$ Uncorrected for Nuclear Absorption
Table IB	17.5 Mev	1.9	1.13	1.02	1.19	2.6×10^{-30}	$\pm 0.3 \times 10^{-30}$	
$p + C \rightarrow \pi^+$	34.0	3.3	1.09	1.06	1.19	4.5	0.4	
	40.2*					8.5	1.1	
	54.0*					13.3	1.2	
	66.5*					12.3	1.4	
	70.0	9.2	1.06	1.24	1.02	12.3	1.4	
	74.0*					12.3	1.2	
Table IC	17.5					0.6	0.3	0.6
$p + p \rightarrow \pi^+$	34.0					1.2	0.4	1.1
	60.9					2.4	0.9	2.0
	63.8					1.6	1.0	1.3
	65.7					2.9	1.3	2.4
	67.2					9.0	1.3	7.4
	68.8					24.3	1.4	20.0
	70.7					27.7	1.5	22.3
	72.3					6.5	1.4	5.1
	73.5					1.5	1.2	1.2
	75.6					1.4	1.2	1.0

*Data of Merritt and Schulz

V. DISCUSSION

Two possible reactions can occur in this experiment:

$$p + p \rightarrow \pi^+ + n + p. \qquad (A)$$

$$p + p \rightarrow \pi^+ + d. \qquad (B)$$

At maximum meson energy the proton and neutron possess the same velocity and a deuteron may be formed.

The maximum meson energy is determined by the proton beam energy, the meson mass, and the total mass of the resulting nucleons. If a deuteron is formed, its binding energy is available to the reaction and the maximum meson energy is, in the laboratory system, 4 Mev higher than for no deuteron formation. (The dynamics of the "two body" problem at maximum meson energy are discussed in Appendix 2.)

Thus, if the products of the reaction are a meson, a proton, and a neutron, then the meson energy spectrum will consist of a continuum from 0 Mev to the maximum meson energy attainable in reaction (A). If a deuteron is formed, the spectrum will contain, in addition, a line 4 Mev above the cut-off in the continuum.

Initial experimental results showed a strong peak near the upper limit of the meson energy spectrum[3,5]. This led to the suggestion made by Brueckner, Chew, and Hart[7] that the wave function of the final nucleon system must strongly affect the meson spectrum. This wave function, dependent as it is on the relative momentum of the two final nucleons, is a rapidly varying function of the energy of the meson near the maximum meson energy. The development of this idea by Brueckner and Watson[8] led to a phenomenological theory which predicted spectra in good agreement with the experimental results. A complete discussion of their treatment of the problem is given in their paper.

In this treatment an expression is obtained for the production cross-section

in terms of the final wave function of the nucleon-nucleon system evaluated at the system's center of mass, $\psi_F(o)$, a factor proportional to the momentum space available to the resulting particles, dJ, and, in addition, a series of terms involving the meson momentum, p, and the angle of production, θ, in the nucleon-nucleon-meson center of mass system. (These last terms correspond to the various wave states of the meson.)

$$d\sigma = dJ \left| \psi_F(o) \right|^2 \left[A + Bp^2 + Cp^2 \cos^2\theta + \text{-----} \right]. \qquad (27)$$

The contribution of the various possible final nucleon-nucleon wave functions, $\psi_F(o)$, and of each of the terms in the meson momentum expansion is to be determined by this and other meson production experiments.

The outstanding feature in the spectrum of mesons produced at zero degrees by protons on protons which such a theory has to explain, is the intense peak near maximum meson energy. The shape of the spectrum near the peak is primarily determined, in the theory, by the final nucleon wave function. In order for such a peak to result it is necessary that the final nucleons be in an S state, either triplet or singlet.

If the resulting nucleons are produced into a ^3S state, then according to Brueckner and Watson, meson production will be accompanied by deuteron formation for a large percentage of the time. The line resulting from the deuteron formation will be intense compared to the continuum, thus explaining the peak. Fig. 6A shows a typical theoretical spectrum for the nucleons produced into the ^3S state.

If the nucleons are left in the ^1S state, a strong peak will still arise because of the resonance resulting from the low energy virtual state. This peak occurring at the cut-off in the continuum would be 4 Mev lower than the line which results if a deuteron is formed. Fig. 6B shows a typical spectrum for this case.

It can be concluded from the results of this experiment that the peak in the spectrum is due solely to deuteron formation. In order to arrive at this conclusion, it was necessary to make an estimate of the resolution of the apparatus. (The resolution is discussed in Appendix 3 .) The resolution was folded into the theoretical spectra of Brueckner and Watson, and the resulting curves were compared with the experimental points.

Fig. 7, curve II, shows the result of folding the resolution into that spectrum in which the nucleons are left in the ^1S state, and the mesons are produced into a P state with a $\cos^2$ distribution in the center of mass system, (the third term in Eq. (27)). As mentioned above, the shape of the spectrum at the peak is primarily determined just by the final nucleon state. This choice for the meson wave state, however, gives the best fit, of the ^1S nucleon theoretical spectra, to the experimental points near the peak.

Fig. 7, curve I, shows the result of folding the resolution into that spectrum in which the nucleons are left in the ^3S state, and the mesons are again produced into a P state with a $\cos^2$ distribution. Since the main feature of this spectrum is a line displaced upward by 4 Mev from the continuum, this curve is essentially a plot of the estimated resolution. (The resolving power is sufficiently high, as is shown in Appendix 3 , that the apparatus does not appreciably mix the continuum and the line spectrum.) The selection of the particular momentum and angular distribution of the meson is even less critical here than for the ^1S case, since the intense deuteron peak is the essential feature of all the ^3S spectra.

Fig. 7 also shows the experimental points. Both theoretical curves are normalized so that the area from 65.5 Mev to 76.0 Mev agrees with the area under the experimental points in the same energy interval. The close fit of curve I with the experimental results is strong evidence that the peak corresponds to

deuteron formation. It is clear that the experimental points, on the other hand, are not in agreement with either the half-width or the assymetric character of curve II for the ^1S case.

The experimental results thus establish that the peak is largely due to deuteron formation. There is still the possibility to be examined that the peak contains an appreciable contribution from ^1S final nucleon states. However, the singlet S peak contribution will occur 4 Mev below the contribution from the triplet S deuteron line. Since, as mentioned above, the resolving power of the apparatus is high enough to distinguish details in the spectrum that are 4 Mev apart, any appreciable singlet S contribution would have occured in the experimental results as a separate peak 4 Mev below that of the deuteron. Therefore, it can be said that the intense peak is due entirely to deuteron formation.

Since the peak accounts for approximately 70 percent of the total cross section at 0°, it is clear that at least 70 percent of the mesons produced at 0° are accompanied by nucleons in the ^3S state. Information from the peak alone, however, is not sufficient to determine the wave states into which the mesons are produced. It might be expected that the lower energy portion of the experimental spectrum could help determine the contribution from each of the meson and nucleon wave states. Final nucleon states other than ^3S could contribute to $\psi_F(o)$ in Eq. (27) at energies in the continuum. (The solid curve in Fig. 5 shows the theoretical curve, with the resolving power folded in, assuming that all of the mesons are produced in the P state with a $\cos^2$ distribution accompanied by nucleons in the ^3S state.) There are two factors that make analysis of the continuum difficult. First, since several angular momentum states of the final nucleon system can contribute to $\psi_F(o)$, there are many possible $\psi_F(o)$ which, taken with various values for the constants in Eq. (27), result in theoretical spectra which agree with the slowly varying continuum that was found experimentally. Second, since a CH_2 - C subtraction method was used,

the low production cross section from hydrogen at low energies resulted in poorer statistics in this region than at the peak. A more sensitive method of determining the coefficients of the various terms in the phenomenological theory would be an investigation of the production cross-section at other angles[4,5,6] and for other proton beam energies.*

(A region of the spectrum not investigated is that between 0 Mev and 15 Mev, where the high background and low cross-section for meson production made scanning too difficult to be reliable. In this region, however, a departure from the flat character of the low energy spectrum is possible. At the maximum meson energy, the two nucleons have a very small relative velocity thus leading to the large peak. Similarly, at about 15 Mev, the meson and one nucleon have low relative velocity. If a large attractive interaction exists between meson and nucleon, the wave function of the two particles will be "bunched" near their center of mass, in a manner analagous to the proton-neutron bunching at maximum meson energy, and thus an increase in cross-section is possible.

VI. MESON MASS DETERMINATION

The sharp peak in the meson energy spectrum at maximum energy provides a method of measuring the π^+-meson mass, since the meson energy at the peak depends only on the meson mass, the proton beam energy, and the total mass of the resulting nucleons. (See Appendix 2 on dynamics.)

As was shown in the preceding section, the peak results from deuteron formation. Therefore, the total mass of the resulting nucleons to be used in the mass determination must be that of the deuteron. One needs, then, only the energy of those mesons which are accompanied by deuteron formation and the proton beam energy in order to determine the meson mass, using the dynamics of Appendix 2.

---

* A. Schulz and J. Merritt are at present measuring the production cross-section at lower proton energies.

The energy of the mesons in the deuteron peak was found by locating the energy at which the deuteron line spectrum must occur in order that the experimental points agree with the curve obtained by folding the experimental resolution into the theoretical spectrum. Any of the ^3S spectra by Brueckner and Watson (see Section V) will, after the resolution is folded in, fit the experimental points at the peak if the line spectrum resulting from deuteron formation occurs at 70.6 Mev.*

The proton beam energy was measured from its Čerenkov radiation by Mr. R. L. Mather[17]. The beam energy measurements, made immediately before and after the bombardment of the target, did not differ perceptibly. Since the cyclotron controls were not disturbed during the run, it was assumed that the beam energy was constant in time. This energy, measured just beyond the snout of the collimator of the external proton beam, was 341.3 Mev ± about 1 Mev. During the bombardment of the CH_2 target, an ion chamber, used for the integration of the beam, was interposed between the snout and the target. The beam of original energy 341.3 Mev travelled through the ion chamber, and in addition, through about one meter of air before striking the CH_2 target. The energy of the beam impinging on the target was 340.4 ± 1.0 Mev.

With this proton energy and the value of 70.6 Mev for the peak energy at which the mesons are produced, the meson mass is determined to be 275.1 ± 2.5

* It is to be noted that the experimental peak occurs at 70.0 Mev in Figs. 5 and 7, rather than at 70.6 Mev, the energy at which the mesons are produced. This apparent discrepancy arises because the energy of each of the experimental points plotted in Figs. 5 and 7 was determined from the range-energy curves under the assumption that the mesons did not undergo small angle scattering in reaching the end of their range. In the estimation of the resolution (Appendix 3), the scattering has been taken into account. Thus, the solid curve of Fig. 5, which results from folding the resolution into a ^3S spectrum with the deuteron line located at 70.6 Mev, exhibits a peak shifted down to 70.0 Mev. Since the method of determining the resolution is approximate, this shift in the peak position is uncertain to an estimated 30 percent.

electron masses.

The estimated errors contributing to the uncertainty in the mass measurement are given in Table II. The source of the error is given in Column I. The estimated error is given in Column II. And the resultant error in the meson mass is given in Column III.

TABLE II. ESTIMATED ERRORS IN MESON MASS DETERMINATION

Source of Error	Estimated Error in Source	Resultant Error in m_π (in electron masses)
Measurement of range in absorbers	± 2% in range or ± 0.8 Mev in meson energy	± 1.0
Uncertainty in range-energy curves	± 1 Mev in meson energy	± 1.2
Shift of peak due to scattering	± 0.2 Mev in meson energy	± 0.24
Fit of theoretical curve to experimental points	± 1 Mev in meson energy	± 1.2
Proton beam energy	± 1 Mev in proton energy or ± 0.9 Mev in meson energy	± 1.1

VII. ACKNOWLEDGMENTS

It is a great pleasure to acknowledge the help and encouragement of Professor C. Richman. Many stimulating discussions were also held with Professor H. A. Wilcox and Drs. K. M. Watson and M. Skinner.

The planning and execution of the experiment in its early stages were made in cooperation with Miss M. N. Whitehead.

I am indebted to R. L. Mather who kindly made the beam energy measurements necessary for the meson mass determination, and to A. Schulz and J. Merritt for

permission to quote their results prior to the publication of their paper.

This work was done under the auspices of the Atomic Energy Commission.

VIII. APPENDICES

APPENDIX 1. SOLID ANGLE CALCULATION

In this section those aspects of magnetic focussing are investigated which affect the calculation of the solid angle subtended at the target by unit area at the emulsion. Although the focussing properties of magnetic fields are well known, considerable space will be taken here to derive the expressions which are most useful in this calculation.

A. In a Uniform Magnetic Field

The solid angle subtended at the target by a unit area normal to the trajectory can be calculated easily for the case in which the trajectory lies entirely in a uniform magnetic field. In Fig. 8 a plan view is shown of two trajectories for two equal momentum mesons in a uniform magnetic field which is perpendicular to the figure. The trajectories originate at point A, the target, and terminate at points B and C, where C is so chosen as to lie on the radius OB. The length Δu, equal to BC is nearly perpendicular to both trajectories for small values of Δu. The tangent at A to the arc AB makes an angle $\Delta\theta$ with the tangent at A to the arc AC. The distance Δu thus subtends an angle in the horizontal plane of $\Delta\theta$ at the point A.

To determine Δu in terms of $\Delta\theta$, we have,

$$\Delta u = \rho - (\rho - v \sin\varphi) \cos \beta. \tag{28}$$

Now, to first order,

$$v = \rho\Delta\theta \qquad \text{and } \cos \beta = 1 . \tag{29}$$

So,

$$\Delta\theta = \frac{\Delta u}{\rho \sin\varphi} . \tag{30}$$

The vertical angle, $\Delta\alpha$, in the solid angle, $\Delta\alpha\ \Delta\theta$, is related to a vertical distance Δz, in the usual way, since the magnetic field does not distort the trajectories in the vertical direction. Thus, (see Fig. 9)

$$r\Delta\alpha = \Delta z. \tag{31}$$

Since the distance r equals the length of the trajectory $\rho\varphi$,

$$\Delta\alpha = \frac{\Delta z}{\rho\varphi}. \tag{32}$$

Thus, the solid angle per unit area is

$$\frac{d\Omega}{dA} = \frac{\Delta\alpha\ \Delta\theta}{\Delta z\ \Delta u} = \frac{1}{\rho^2\varphi\sin\varphi}\ \frac{\text{ster.}}{\text{cm}^2}.* \tag{1}$$

B. Corrections

Corrections must be made to Eq. (1) because the nuclear emulsions were not located in the uniform field, but were placed just outside of the magnet gap in the fringing field. Eq. (30) is now clearly incorrect, since the trajectories are no longer circular from beginning to end. In addition, because of the nature of a magnetic field, there are fringing field forces that further distort the trajectories. These corrections can be determined by examining the expression for the Lorentz force on a meson in a fringing magnetic field.

Consider a semi-infinite field such as is shown in Fig. 10. This is a good approximation to the actual field at the pole face edge. In a current free region, curl $\vec{H} = 0$. Since the field is semi-infinite, H_x and H_z do not change in the y direction and we have

$$\frac{\partial H_x}{\partial y} = \frac{\partial H_y}{\partial x} = 0;\quad \frac{\partial H_z}{\partial x} = \frac{\partial H_x}{\partial z};\quad \frac{\partial H_z}{\partial y} = \frac{\partial H_y}{\partial z} = 0. \tag{33}$$

* In deriving Eq. (1), it has been assumed that the trajectories are all very nearly in a plane perpendicular to the lines of force. This was implied by setting r equal to $\rho\varphi$ in Eq. (32) and also in deriving Eq. (30). It can be easily shown, however, that for all possible trajectories from target to emulsion in this experiment, corrections because of the vertical component of the motion are only of the order of 0.1 percent.

Therefore, since H_x is zero at $z = 0$ (the median plane), at a small distance Δz above that plane,

$$H_x(\Delta Z) = \frac{\partial H_x}{\partial Z}\Delta Z = \frac{\partial H_z}{\partial x}\Delta Z;\ H_y = 0;\ H_z = H_z\ (x). \tag{34}$$

So, since $\vec{F} = (\vec{v} \times \vec{H})e/c$, the components of the force on a meson leaving the gap at Δz are:

$$F_x = (-v_z H_y + v_y H_z)\frac{e}{c} = \frac{e}{c} v_y H_z \tag{35a}$$

$$F_y = (-v_x H_z + v_z H_x)\frac{e}{c} = \left(-v_x H_z + v_z \frac{\partial H_z}{\partial x}\Delta Z\right)\frac{e}{c} \tag{35b}$$

$$F_z = (-v_y H_x + v_x H_y)\frac{e}{c} = -\frac{e}{c} v_y \frac{\partial H_z}{\partial x}\Delta Z \tag{35c}$$

Now $\frac{e}{c} v_x H_z$ and $\frac{e}{c} v_y H_z$ are the components of the Lorentz force already considered implicitly in obtaining the relation (30): $\Delta\theta = \frac{\Delta u}{\rho \sin\varphi}$. But, since H_z decreases at the gap edge, this formula no longer holds. The correction to Eq. (1) because of these two terms will be taken up later.

First, we consider the other two terms in the Lorentz force

$$F_z = -\frac{e}{c} v_y \frac{\partial H_z}{\partial x}\Delta Z \tag{35c}$$

and, from Eq. (35b)

$$F_y = \frac{e}{c} v_z \frac{\partial H_z}{\partial x}\Delta Z. \tag{36}$$

The first of these gives rise to the "thin lens" formula, as is shown here. Consider a trajectory leaving the magnetic field. (See Fig. 11.) It is assumed that the field goes from H_o to zero in a distance small compared with the trajectory length. (See Fig. 12.) (This assumption will be discussed later.) It can then be shown that the region in which the field drops to zero acts, for each vertical plane, like a lens with a focal length $f = \frac{-\rho}{\tan\delta}$,

for those trajectories originating on the median plane. ρ is the radius of curvature of the trajectories in the uniform magnetic field, and δ is the angle the vertical plane makes with that particular vertical plane which is normal to the gap edge. Since the target extends above and below the median plane, however, all the trajectories clearly do not originate in this plane. It becomes necessary, therefore, to find the quantity which corresponds to the focal length, as shown below.

The change in momentum due to the force $F_z = \frac{e}{c} v_y \frac{\partial H_z}{\partial x} \Delta Z$ occurs, according to the above assumption, only in the region between ℓ_1, and ℓ_2 (Fig. 12). This momentum change is

$$\Delta p_z = \int F_z \, dt = \int_{\ell_1}^{\ell_2} F_z \frac{dx}{v_x} . \tag{37}$$

Since,

$$F_z = - \frac{e}{c} v_x \tan\delta \frac{\partial H_z}{\partial x} \Delta Z, \tag{38}$$

then,

$$\Delta p_z = - \frac{e}{c} \Delta Z \tan\delta \int_{H_o}^{o} dH_z . \tag{39}$$

Now, (see Fig. 13)

$$p_z \cong - p \frac{(\Delta Z)'}{a} . \tag{40}$$

And with $\rho = \frac{pc}{eH}$, this yields $\frac{\Delta p_z}{p_z} = - \frac{a \tan\delta}{\rho} \frac{\Delta Z}{(\Delta Z)'}$. (41)

Thus,

$$p_z' = p_z + \Delta p_z = p_z \left(1 - \frac{\Delta Z}{(\Delta Z)'} \frac{a}{\rho} \tan\delta\right) . \tag{42}$$

After passing through the fringing region, the particle which starts at a point that is a distance b above the median plane and a distance a from the gap edge moves as though from a point t. (See Fig. 13.) From Fig. 13, it can

be shown that

$$\frac{1}{a} - \frac{1}{t} = \frac{1}{a}\left(1 - \frac{\varepsilon}{\alpha'}\right) \quad \text{and} \quad \frac{\varepsilon}{\alpha'} = \frac{p_z'}{p_z}. \tag{43}$$

Therefore,

$$\frac{1}{a} - \frac{1}{t} = \frac{1}{a}\left[1 - \left(1 - \frac{\Delta Z}{(\Delta Z)'}\,\frac{a \tan\delta}{\rho}\right)\right] \tag{44}$$

$$= \frac{\tan\delta}{\rho}\left(\frac{b - a\alpha'}{a\alpha'}\right) = \frac{1}{g}.$$

The quantity g corresponds to a "focal length" since the "object distance", a, and the "image distance", t, are related to it by the thin lens equation. g becomes a true focal length when the trajectory originates on the median plane ($b \to 0$).

This "focal length", g, is now used to determine the relation between the increment of angle, $\Delta\alpha'$, subtended at the target by a small vertical distance, $\Delta\zeta$, at the position of the emulsion.

From Fig. 13,

$$\alpha' = \frac{b - \zeta}{a}\,\frac{1}{1 + x\left(\frac{1}{a} - \frac{1}{g}\right)}. \tag{45}$$

So,

$$b - \zeta = \rho\varphi\alpha'\left(1 + \frac{x}{\rho\varphi} + \frac{x \tan\delta}{\rho}\right) - x\,\frac{(\tan\delta)b}{\rho}. \tag{46}$$

Therefore,

$$\Delta\alpha' = \frac{\Delta\zeta}{\rho\varphi + x(1 + \varphi \tan\delta)}, \tag{47}$$

where φ is the angle through which the tangent to the trajectory turns from the target to the pole face edge. This reduces to Eq. (32) when $x = 0$.

Next, we consider the second of the fringing terms. (See Eq. (36).) $F_y = v_z \frac{\partial H_z}{\partial x}\,\Delta Z\,\frac{e}{c}$ produces a distortion of the trajectories in the horizontal plane. If, as above, we calculate the change in momentum resulting from this

force, we obtain

$$\Delta p_y = -\frac{v_z}{v_x} H_o \, \Delta Z \, \frac{e}{c} = - p_z \frac{\Delta Z}{\rho} \quad . \tag{48}$$

The displacement of the trajectories resulting from this momentum change is shown in Fig. 14. The trajectories OA' and OB' cross the gap edge at the same distance above the median plane. Thus, the Δp_y of the mesons travelling along OA' and OB' are the same, and the distance A'B' is equal to the distance AB. It is also easily shown that the distances A'C' and AC, perpendicular to the trajectories, are equal to within a few hundredth of a per cent. The fringing forces, then, produce no change in $\frac{\Delta\theta}{\Delta u}$, even though the trajectories are distorted. We can therefore neglect $F_y = \frac{e}{c} v_z \frac{\partial H_z}{\partial x} \Delta Z$ in determining corrections to the solid angle relation.

The correction to Eq. (30) because of the decrease in H_z in the terms $\frac{e}{c} v_x H_z$ and $\frac{e}{c} v_y H_z$ is now calculated. These two terms, as mentioned above, are the components of the Lorentz force considered in deriving the equation for the solid angle in a uniform field.

The trajectories of the mesons as they left the magnetic field made an angle δ of about 5 degrees with the normal to the gap edge. Fig. 15 illustrates this. It is assumed again that the field is uniform to the pole face edge and is zero beyond. Then upon reaching the pole face edge, the trajectory becomes the tangent to the circle. Since the trajectory OBA has more of its length in the field than OC, the non-perpendicular exit produces a focussing effect.

We now find the angle, $(\Delta\theta)'$, between the trajectories as they leave the target, as a function of the distance between them, Δu, outside the field at a distance, x, from the pole face edge.

We see from Fig. 15 that

$$\omega = \Delta\varphi - \beta \; . \tag{49}$$

Now,

$$\Delta\varphi = \frac{\ell \sin\delta}{\rho} = \sin\varphi \tan\delta \, (\Delta\theta)' \tag{50}$$

since

$$\ell \cos\delta = d = \rho(\Delta\theta)' \sin\varphi . \tag{51}$$

And (see Fig. 8)

$$\beta = (\Delta\theta)' \cos\varphi . \tag{52}$$

Therefore

$$\omega = (\Delta\theta)' \, (\sin\varphi \tan\delta - \cos\varphi). \tag{53}$$

But,

$$\Delta u = \omega \, (z - x) = d - \omega x = (\Delta\theta)' \, \rho \sin\varphi - \omega x \tag{54}$$

since

$$d = \omega (z + y) \cong \omega z . \tag{55}$$

So finally

$$\Delta u = (\Delta\theta)' \, (\rho \sin\varphi - x \sin\varphi \tan\delta + x \cos\varphi) \tag{56}$$

or

$$\frac{(\Delta\theta)'}{\Delta u} = \frac{1}{\rho \sin\varphi - x \sin\varphi \tan\delta + x \cos\varphi} . \tag{57}$$

With $x = 0$, i.e. no change in field along the trajectory, this reduces to (30).

The solid angle per unit area, corrected for the fringing field and the non-perpendicular exit of the meson from the field gap, is, after substituting from Eqs. (47) and (57)

$$\frac{(\Delta\theta)' \, (\Delta\alpha)'}{\Delta u \, \Delta\zeta} = \frac{1}{(\rho\varphi + x) \left[1 + (\varphi \tan\delta)\left(\frac{x}{\rho\varphi + x}\right)\right] \left[\begin{array}{l}\rho \sin\varphi + x \cos\varphi \\ - x \sin\varphi \tan\delta\end{array}\right]} . \tag{58}$$

The value of x used in the experimental arrangement was approximately 2 inches, while ρ was about 14 inches. δ was about 5 degrees, and consequently $\tan\delta$ had a value of about 0.1. Expanding the right-hand side of Eq. (58), and neglecting terms of the order of $x^2 \tan\delta$ compared to terms of the order of ρ^2,

we obtain a relation for the solid angle, which for the experimental dimensions is accurate to better than 1 percent:

$$\frac{d\Omega}{dA} = \frac{1}{\rho^2 \left(\varphi + \frac{x}{\rho}\right)(\sin\varphi)\left[1 + \frac{x}{\rho}\cot\varphi\right]} . \tag{2}$$

This expression is identical to the formula $\frac{1}{\rho^2\varphi' \sin\varphi'}$ (for small x/ρ) where $\varphi' = \varphi + \frac{x}{\rho}$. Thus, if one assumed that the uniform field extended to the emulsion, the result would be accurate to first order in x/ρ, (or to within 2 percent here). This was all derived on the basis that the field dropped to zero in a very small distance. However, since the field actually does not drop to zero in a distance short compared to x, the above expression is accurate to better than 2 percent.

The reason that the effect of the drop off in magnetic field is so small is that, although the vertical field, H_z, which produces the focussing inside the region of the uniform field decreases near the gap, the fringing forces resulting from curl $\vec{H} = 0$ produce a focussing action which for small x/ρ exactly compensates for this decrease in H_z.

It can also be shown that the change in the solid angle due to the loss in energy in the absorber is negligible.

APPENDIX 2. DYNAMICS

At the maximum meson energy, the product nucleons, neutron and proton, have the same velocity, and the dynamics become simply those for the two body problem. The momentum and energy balance equations for this problem were solved, giving the γ_π of the meson in the laboratory system in terms of the proton beam γ_p, the total mass of the resulting nucleons, the mass of the meson, m_π, the proton mass, m_p, and the angle φ at which the meson is produced in the laboratory system.

$$\gamma_\pi = \frac{\Delta - 2r(\gamma_p+1) \pm 2\cos\varphi\sqrt{(\gamma_p^2-1)(r^2-1) + \cos^2\varphi(\gamma_p-1)^2 - (\gamma_p-1)r\Delta + \frac{\Delta^2}{4}\left(\frac{\gamma_p-1}{\gamma_p+1}\right)}}{-2\left(\sin^2\varphi\,(\gamma_p-1) + 2\right)} \tag{59}$$

where, if T is the kinetic energy in the laboratory system, $\gamma_\pi = 1 + T_\pi/m_\pi c^2$, $\gamma_p = 1 + T_p/m_p c^2$, $\Delta = \frac{m_F^2 - m_\pi^2}{m_p\, m_\pi}$, m_F is the total combined mass of the final nucleons, and $r = m_p/m_\pi$.

Using Eq. (59), the dependence of the maximum meson energy on various parameters has been calculated under the assumption that m_F is the deuteron mass.

The maximum meson energy is plotted as a function of angle of production in Fig. 16.

For mesons of 275.1 electron masses, and 340 Mev protons, the change in maximum meson energy due to a change in proton energy is

$$\frac{dE_\pi}{dE_p} = 0.91. \tag{60}$$

For 340 Mev protons the change in the maximum meson energy with meson mass is, in the vicinity of 275.1 electron masses, given by

$$\frac{dE_\pi}{dm_\pi} = 0.83\ \mathrm{Mev}/m_e. \tag{61}$$

These calculations assumed the nucleons to be in a bound state, with m_F equal to the deuteron mass. If, instead, we take m_F to be the sum of neutron and proton masses, the maximum meson energy is obtained for the case of no deuteron formation. For 275.1 electron mass mesons and 340 Mev protons, this energy is 66.12 Mev. The difference between the maximum energies with and without deuteron formation is thus 70.28 - 66.12 = 4.16 Mev.

APPENDIX 3. RESOLUTION

The experimental energy spectrum of the mesons was determined from the density of meson endings found at each depth in the absorber. The density of mesons as a function of range was then converted to the density of mesons as a function of energy by means of the range-energy curves for mesons. This de-

tection method introduces a finite resolving power into the apparatus. Mesons of a particular energy will not have a unique depth of penetration into the absorber because of range straggling and multiple small angle scattering. The first effect is due to the statistical fluctuations in the number of collisions the meson undergoes, and gives a gaussian distribution in range. The Williams' scattering gives rise to a distribution in depth of penetration for mesons of the same range because the projected range depends on the angles through which each meson has been scattered in the course of its travel through the absorber. Since the energy of a meson was deduced from the position of its ending in the absorber, the above variation in depth of penetration for a monoenergetic beam of mesons will manifest itself as an apparent spread in the energies of the mesons coming into the absorber.

Further energy smearing might arise because the detector accepts mesons from a small range of angles about zero degrees, and the meson cut-off energy or peak energy, in which we are interested, varies with the angle of production. The effect of this angular spread in mesons accepted by the detector can be calculated for maximum energy mesons quite easily, since the dynamics of the production process are then straightforward (see Appendix 2) and the simple geometry is amenable to precise measurement. Fig. 16 shows that the maximum meson energy produced in the proton-proton interaction changes very slowly as the angle of production is varied about 0°. The geometry of the experiment allowed a variation in angle, for the maximum energy mesons, from -3° to $+3^{\circ}$, which corresponds to a spread in energy of less than 0.2 Mev. Therefore, this effect can be neglected in determining the resolving power.

The use of a thick target would also be expected to decrease the resolving power. As is shown in Appendix 4, however, for this particular reaction, $p + p \rightarrow \pi^{+}$, the effect of the finite target thickness on the resolution is

negligible, for maximum energy mesons.

Thus, the main causes of the finite resolving power introduced by the detection method are the multiple small angle scattering and the range straggling mentioned above. An additional energy spread is introduced into the experiment by the proton beam, which is itself not monoenergetic. The energy distribution of maximum energy mesons because of each of these three effects has been calculated below. The three distributions are then folded together. The resulting curve, shown in Fig. 19C, gives the distribution in energy that maximum energy mesons produced in proton-proton collisions will be observed to have when produced and detected with the experimental equipment used.

The resolution has been assumed to be constant over the high energy part of the spectrum in obtaining the curves in Fig. 7.

The depth of penetration for a monoenergetic beam of mesons entering an absorber normally will have a distribution, due to scattering, which is calculated below approximately.

The distribution in angle that a collimated monoenergetic beam of mesons will possess after passing through an absorber of thickness dx is gaussian with a mean square angular spread given by the expression[18]

$$\theta^2_{rms} = \frac{8\pi\, N z^2 Z^2\, e^4\, dx}{v^2\, p^2} \ln \frac{a_o\, vp}{2Z^{4/3}\, z\, e^2} \tag{62}$$

where N is the number of atoms per cubic centimeter of the absorber, z is the charge on the meson in electronic charge units, Z is the atomic charge of the absorber material, e is the electronic charge, a_o is the Bohr radius, and v and p are the velocity and momentum of the mesons.

If Eq. (62) is written as

$$\theta^2_{rms} = \frac{Z}{m_\pi/m_e} \frac{dE}{dx} \mathcal{L}(E) \frac{dx}{E} \tag{63}$$

where m_π and m_e are the masses of the meson and electron and dE/dx is the rate of energy loss of mesons in the absorber, then the factor $\mathcal{L}(E)$ is a slowly varying function of E, the kinetic energy. This factor is plotted in Fig. 17 for aluminum. (Within a few percent, $\mathcal{L}(E)$ has the same values for copper as for aluminum.)

Now the originally collimated beam becomes more and more spread out in angle as it passes through the absorber. The additional spread it receives in each dx is independent of the scattering it received in the previous dx's. Consequently, the resultant distribution in angle at any depth x will be a gaussian of mean square angular displacement equal to the sum of the mean square displacements of all dx's from x = 0 to x = x. This is expressed as

$$\Theta^2_{rms}(x) = \sum \theta^2_{rms}(x) = \int_0^x \frac{Z}{m_\pi/m_e} \frac{dE}{dx} \mathcal{L}(E) \frac{dx}{E} \tag{64}$$

where $\Theta^2_{rms}(x)$ is the accumulated mean square angle and Eq. (63) has been used for $\theta^2_{rms}(x)$. Selecting from the plot of the slowly varying function $\mathcal{L}(E)$ the mean value of 1.2, and making use of Eq. (15), we get for $\Theta^2_{rms}(x)$:

$$\Theta^2_{rms}(x) = \frac{0.68}{m_\pi/m_e} Z \ln\left(\frac{1}{1 - x/R_o}\right). \tag{65}$$

It might be noted that, according to Eq. (65), $\Theta^2_{rms}(x)$ depends, not on the energy or total range, but only on the fraction of the range already covered. Actually this is not strictly true, and arises from taking $\mathcal{L}(E)$ equal to a constant. In the energy interval in question (0 to 70 Mev), $\mathcal{L}(E)$ does not vary by more than 20 percent from the mean value used. Eq. (62), and therefore Eq. (65), is not applicable near $x = R_o$, since the scattering the meson undergoes at very low energies is no longer small angle scattering. In aluminum, for $x = 0.99\ R_o$, however, Θ_{rms}, as computed from Eq. (65), is about 25°. The

assumption of small angle scattering is therefore valid in the interval $x = 0$ to $x = 0.99\ R_o$. Since almost all of the variation in depth of penetration of the mesons occurs in this interval (see Eq. (72) and Fig. 18), Eq. (65) should be accurate, for our purposes, to within about 20 percent.

Now, in order to obtain the distribution in depth from the expression for $\Theta^2_{rms}(x)$, we introduce the stipulation that a meson at a depth x' whose trajectory makes an angle $\Theta(x')$ with the forward direction, where $\Theta(x') = k\ x\ \Theta_{rms}(x')$, will always, at any x, maintain a direction of travel given by $\Theta(x) = k\ \Theta_{rms}(x)$. Thus, a meson travelling at an angle equal to twice the rms angle, always travels at twice the rms angle. This assumption is not unreasonable for determining a rough idea of the distribution. An exact treatment of the problem is very difficult. On the other hand, the above assumption leads to a distribution in depth of penetration, which seems more realistic than assuming, for example, a constant "average" decrease in depth of penetration for each meson.

Since the distribution in $\Theta(x)$ is gaussian, the distribution in k is also gaussian, and the fraction of the total number of mesons with k in dk is

$$N(k)dk = \frac{2}{\sqrt{2\pi}}\, e^{-k^2/2}\, dk. \tag{66}$$

By specifying the angle with which each meson travels relative to the original direction we are able to compute each path. The path length is given by

$$S = \int_0^s ds = \int_0^x \frac{dx}{\cos\Theta(x)} \tag{67}$$

since $ds = dx/\cos\Theta(x)$. The depth of penetration, or projected path distance, is x. So, the shortening, $w(x)$, in projected path distance due to

scattering is

$$w(x) = s - x = \int_0^x dx \left(\frac{1}{\cos \Theta(x)} - 1\right) . \tag{68}$$

For small Θ this becomes

$$w(x) = \int_0^x \frac{\Theta^2(x)}{2} dx. \tag{69}$$

The meson which maintains the rms angle thus has a shortening of projected path distance, at the depth x, given by

$$w^*(x) = \int_0^x \frac{dx}{2} \left[\frac{.68}{m_\pi/m_e} Z \ln \frac{R_o}{R_o - x}\right] . \tag{70}$$

Upon integrating, this becomes

$$w^*(x) = \frac{0.34}{m_\pi/m_e} R_o Z f\left(\frac{x}{R_o}\right); \tag{71}$$

where

$$f\left(\frac{x}{R_o}\right) = \left(1 - \frac{x}{R_o}\right) \ln \left(1 - \frac{x}{R_o}\right) + \frac{x}{R_o} . \tag{72}$$

$f(x/R_o)$ is plotted in Fig. 18.

The meson maintaining the direction of travel $k\,\Theta_{rms}$ has, then a decrease in depth of penetration $w(x) = k^2 w^*(x)$. The distribution in w is then found from the distribution in k.

$$N(w)\, dw = N(k)\, dk. \tag{73}$$

Thus

$$N(w)\, dw = \frac{e^{-\frac{w}{2w^*}}}{\sqrt{2\pi w^* w}} dw . \tag{74}$$

This distribution is a function of x since w^* is a function of x.

For $x = R_o$, the mesons having travelled their whole range,

$$w^*(x=R_o) = \frac{0.34}{m_\pi/m_e} R_o Z. \tag{75}$$

The experimental arrangement consisted of a copper absorber of thickness 1.36 cm placed in front of an aluminum absorber in which the nuclear emulsions were embedded. In order to determine the shortening in depth of penetration due to Williams' scattering for mesons of 68.7 Mev (the energy with which the mesons enter the absorber), we first determine the w^*_{cu} the mesons acquire in passing through 1.36 cm ($= 0.55\ R_o$) of copper. From Eq. (71),

$$w^*_{cu} = \frac{0.34}{m_\pi/m_e} R_{o_{cu}} (68.7 \text{ Mev.}) Z_{cu}\ f(0.55) = 0.017 \text{ cm.} \tag{76}$$

The "rms meson" will therefore have an energy, when it reaches the interface, which is lower by an amount ΔE_i than the energy E_i of a meson travelling at 0°, where

$$\Delta E_i = \left.\frac{dE}{dx}\right|_{E_i, cu} w^* . \tag{77}$$

This decrease in energy will manifest itself as a decrease in range in the aluminum given by

$$w^{*\,I}_{al} = \left.\frac{dE}{dx}\right|_{cu, E_i} w^*_{cu} \times \frac{1}{\left.\frac{dE}{dx}\right|_{al,\ E_i}} = 0.048 \text{ cm.} \tag{78}$$

The mesons in travelling through the copper accumulated a gaussian angular distribution with a Θ^2_{rms} (see Eq. (65)) of

$$\Theta^2_{rms} = \frac{0.68}{m_\pi/m_e} Z_{cu} \ln \frac{1}{0.55}. \tag{79}$$

In travelling to the end of their range in aluminum (3.10 cm), the mesons underwent additional scattering. To find the additional projected path shortening,

$w^{*\,II}_{al}$, we note that the same angular distribution at the copper-aluminum interface would have been acquired if the meson had come through a distance x' of aluminum, a fraction of a total range R'_o in aluminum, where x'/R'_o is determined by

$$\Theta^2_{rms}(x'_{al}) = \Theta^2_{rms}(x_{cu}) \tag{80}$$

or

$$\ln\left(1 - \frac{x'}{R'_o}\right) = \frac{Z_{cu}}{Z_{al}} \ln 0.55. \tag{81}$$

From this, $x'/R'_o = 0.83$. R'_o can now be determined since

$$t_{al} = R_o' - x' = R_o'\left(1 - \frac{x'}{R_o'}\right). \tag{82}$$

This yields $R' = 18.2$ cm and $x' = 15.1$ cm. Then from Eqs. (70) and (71)

$$w^{*\,II}_{al} = \int_{x'}^{R_o'} \frac{dx}{2}\left[\frac{0.68}{m_\pi/m_e} Z_{al} \ln\left(\frac{R_o'}{R_o'-x'}\right)\right]$$

$$= \frac{0.34}{m_\pi/m_e} R_o' Z_{al}\left[1 - f\left(x'/R_o'\right)\right]. \tag{83}$$

Substituting the values for R'_o and x', we have $w^{*\,II}_{al} = 0.158$ cm.

The total shortening in depth of penetration is thus

$$w^*_{total} = 0.048 + 0.158 = 0.206 \text{ cm of al.} \tag{84}$$

If then the energy is inferred from the depth of penetration, a meson travelling along the path with the rms Θ will appear to have an energy decreased from the true energy by

$$\Delta E^* = \left.\frac{dE}{dx}\right|_{al} w^*_{total}, \tag{85}$$

where $dE/dx|_{al}$ is the rate of energy loss of mesons of 68.7 Mev in aluminum. This yields, $\Delta E^* = 1.29$ Mev.

The distribution in w will still be given by Eq. (74), with $w^* = 0.206$ cm,

since it has been assumed throughout that any one meson always travels at an angle which is a constant fraction of $\Theta_{rms}(x)$. If the energy of the meson is determined from the depth of penetration, this distribution in w will correspond to an apparent distribution in meson energy such that the fraction of mesons of energy E in dE is given by

$$N(E)dE = \frac{e^{\frac{-(E_o - E)}{2\,(1.29)}}}{\sqrt{2\pi\,(E_o-E)\,(1.29)}}\,dE \tag{86}$$

where E_o is the true meson energy. This distribution is plotted in Fig. 19A as a function of $E - E_o$.

Next, the effect on the energy resolution of range straggling, due to statistical fluctuations in the number of collisions that the meson undergoes, is considered.

Bethe and Livingstone[19] give an expression for the mean square width in the gaussian distribution of distances travelled by particles which lose a given amount of energy by ionization. For mesons of high velocity which decrease in energy from E_1 to E_2 this expression yields

$$\overline{\Delta R^2} = \int_{E_2}^{E_1} \frac{4\pi\, e^2\, N\, Z'}{\left(dE/dx\right)^3}\, dE \tag{87}$$

where e is the electronic charge, N is the number of atoms per cubic centimeter of the absorber, Z' is the number of electrons per atom that are effective in the ionization process, and dE/dx is the rate of energy loss of the meson at the energy E.

The integration can be carried out by means of Eq. (22), $dE/dx = .58\ k\ x\ (R_o - x)^{-.42}$, where R_o is the total range and $R_o - x$ is the residual range.

By integrating the above relation over the meson energy loss in the copper, the ΔR_{rms} incurred by the meson beam in the copper slab was found to be 4.91×10^{-2} cm. This distance in copper corresponds to a distance in aluminum (see

Eq. (78))

$$\Delta R^{I}_{rms}\ (al) = \left(\left.\frac{dE_{II}}{dx}\right|_{cu,E_i} \Big/ \left.\frac{dE_{II}}{dx}\right|_{al,E_i} \right) \times 4.9 10^{-2}\ cm. \qquad (88)$$

The value of the root mean square width in the range distribution incurred in the aluminum was found, similarly, to be

$$\Delta R^{II}_{rms}\ (al) = 7.1 (10^{-2})\ cm. \qquad (89)$$

Since the process by which the ΔR_{rms} accumulates i random, ΔR^{I}_{rms} and ΔR^{II}_{rms} must be added in quadrature. The total accumulated straggling in range is therefore represented by a gaussian with a root mean square width of

$$\Delta R_{rms} = 0.15\ cm\ (al). \qquad (90)$$

If there were no straggling, this gaussian distribution in range would correspond to a gaussian distribution in the energy with which the mesons enter the absorber. The rms spread in this energy distribution is given by

$$\Delta E^2_{rms} = \left(\frac{de}{dx}\right)^2_{al,70Mev} (\Delta R)^2_{rms} = 0.92\ \overline{Mev}^2 \qquad (91)$$

The 340 Mev proton beam has an energy spread estimated to be about 1.5 Mev. Without a detailed analysis of the origin of this spread, it has been assumed that the distribution in energies is gaussian. In the following, an rms spread of 1.2 Mev is used. This value gives the best fit to the experimental points. If, however, any value in the vicinity of 1.5 Mev were used for the rms spread, the conclusions reached in Section V would remain unchanged.

Protons with a gaussian energy distribution will produce mesons whose maximum energy will also have a gaussian distribution. Since a change in proton energy of 1 Mev produces a change of 0.9 Mev in the maximum meson energy (see Eq. (60)), the meson energy gaussian will have an rms width of 0.9 x 1.2 or 1.08 Mev.

The three distributions giving rise to the finite resolving power are, from the above

$$N_1(E)\ dE = \frac{e^{-(E_o-E)/2(1.29)}}{\sqrt{2\ (E_o-E)\ 1.29}}\ dE \tag{92}$$

due to Williams' scattering

$$N_2(E)\ dE = \frac{e^{-(E_o-E)^2/2(.92)}}{\sqrt{2\pi(.92)}}\ dE \tag{93}$$

due to range straggling, and

$$N_3(E)\ dE = \frac{e^{-(E_o-E)^2/2(1.16)}}{\sqrt{2\pi(1.16)}}\ dE \tag{94}$$

due to the proton beam energy width. In these expressions, E_o is the true maximum meson energy produced by 340.4 Mev protons.

The range straggling and proton beam energy distribution, when folded together, give a gaussian of rms width 1.44 Mev. This is plotted in Fig. 19B. The final resolving power curve is found from folding 19A into 19B, and is plotted in Fig. 19C.

APPENDIX 4. THICK TARGET COMPENSATION

Mesons produced at the front of the target lose a small fraction of their energy in traversing the target because of ionization. The proton beam also loses energy in passing through the target, and the maximum energy of the mesons produced at the back of the target is smaller than of those produced at the front. Thus, the ionization loss in the target by the mesons tends to be compensated for by the ionization loss of the protons.

For 340 Mev protons on protons, the ionization loss of the beam, the maximum energy of the created mesons, their rate of energy loss by ionization, and

the rate of decrease of maximum meson energy with proton energy decrease, are such that the maximum energy mesons emerge from the back of the target with the same energy, regardless of their point of origin within the target. This can be shown as follows.

The mesons produced at the front of the target emerge with an energy

$$E_o - \left(\frac{dE_\pi}{dx}\right) \Delta x \tag{95}$$

where dE_π/dx is the rate of energy loss in the target of maximum energy ($\cong$ 70 Mev) mesons. Δx is the target thickness, and E_o is the maximum meson energy for 340 Mev protons.

The protons lose an amount of energy $\Delta E_p = \frac{dE_p}{dx} \Delta x$ in passing through the target, where dE_p/dx is the rate of energy loss in the target for 340 Mev protons.

The peak energy mesons produced by protons of energy $340 - \Delta E_p$ have an energy equal to $E_o - \frac{dE_\pi}{dE_p} \Delta E_p$, where dE_π/dE_p is determined from the dynamics. For 340 Mev protons, $dE_\pi/dE_p = 0.91$. (See Appendix 2.)

Therefore, mesons of maximum energy produced at the back of the target have an energy equal to $E_o - \frac{dE_p}{dx} \frac{dE_\pi}{dE_p} \Delta x$.

For 340 Mev protons, and mesons of mass 275.1 electron masses, $dE_p/dx = 1.16\, dE_\pi/dx$. Therefore, $\frac{dE_p}{dx} \frac{dE_\pi}{dE_p} \Delta x = \frac{1}{0.95} \frac{dE_\pi}{dx} \Delta x$.

The energy of the mesons produced at the front of the target is

$$E_\pi = E_o - \frac{dE_\pi}{dx} \Delta x \tag{96}$$

whereas the energy of the mesons produced at the back of the target is

$$E_\pi' = E_o - \frac{dE_p}{dx} \frac{dE_\pi}{dE_p} \Delta x = E_o - \frac{1}{0.95} \frac{dE_\pi}{dx} \Delta x. \tag{97}$$

Thus, the decrease in energy from E_o is, within 5 percent, the same for all parts of the target.

Fig. 15 Neighboring trajectories in a horizontal plane in a field that drops rapidly from $H = H_o$ to $H = 0$.

Fig. 16 Maximum meson energy as a function of the production angle, in the laboratory system.

Fig. 17 $\mathcal{L}(E)$ as a function of the meson kinetic energy.

Fig. 18 $f(x/R_o)$.

Fig. 19 Distribution in apparent maximum meson energy due (A) to Williams' scattering, (B) to the combined effects of range straggling and proton energy spread, and (C) to all three effects.

For the thickness of CH_2 used, the maximum energy mesons all emerged from the target having, within 0.1 Mev, the same energy. The spread in the meson energy, due to the thick target, is only 0.15 percent.

IX. REFERENCES

1. C. Richman and H. A. Wilcox, Phys. Rev. 78, 496 (1950).
2. M. Weissbluth, UCRL-568 (1950).
3. W. F. Cartwright, C. Richman, M. N. Whitehead, and H. A. Wilcox, Phys. Rev. 78, 823 (1950).
4. C. Richman and M. N. Whitehead. Private communication.
5. V. Z. Peterson, Phys. Rev. 80, 136 (1950).
6. V. Peterson, E. Iloff, and D. Sherman, Phys. Rev. 81, 647 (1951).
7. K. A. Brueckner, Phys. Rev. In press. See Appendix by Brueckner, Chew, and Hart.
8. K. M. Watson and K. A. Brueckner, Phys. Rev. In press.
9. R. R. Wilson, Phys. Rev. 71, 385 (1947).
10. W. A. Aron, B. G. Hoffman, F. C. Williams, AECU-663.
11. R. Mather and E. Segrè, UCRL-1089. Also, Phys. Rev. In press.
12. M. Weissbluth, UCRL-568, Supra, page 22 (1950).
13. O. Chamberlain, R. F. Mozley, J. Steinberger, and C. Wiegand, Phys. Rev. 79, 394 (1950).
14. H. Bradner, F. M. Smith, W. H. Barkas, and A. S. Bishop, Phys. Rev. 77 462 (1950).
15. H. Bradner and B. Rankin, Phys. Rev. 80, 916 (1950).

    G. Bernardini, E. T. Booth, L. Lederman, and J. Tinlot, Phys. Rev. 80 924 (1950).

    M. Camac, D. Corson, R. Littauer, A. Shapiro, A. Silverman, R. Wilson, and W. Woodward, Bull. Amer. Phys. Soc. 26, 48 (1951).

    M. Skinner and C. Richman. Private communication.
16. J. Merritt and A. Schulz, (to be published).

17. R. L. Mather, (to be published).

18. B. Rossi and K. Greisen, Rev. Mod. Phys. 13, 263 (1941). For the particular choice of the log term, see "Nuclear Physics" (Fermi) Revised, 1950, page 37.

19. M. S. Livingstone and H. A. Bethe, Rev. Mod. Phys. 9 283 (1937).

X. FIGURE CAPTIONS

Fig. 1 Schematic diagram of a typical experimental arrangement.

Fig 2 Absorber-detector. (A) With top removed. (B) As used at high meson energies.

Fig. 3 Meson beam impinging on an emulsion embedded in an absorber.

Fig. 4 Target followed by an infinite "sea" of target material.

Fig 5 Plot of the differential cross-section for the process $p + p \rightarrow \pi^+$, at zero degrees, as a function of energy. The solid curve results from folding the experimental resolution into the theoretical spectrum (see Section V) for the final nucleons in a ^3S state and the meson in a P state with a $\cos^2 \theta$ angular distribution.

Fig 6 (A) Theoretical spectrum for the final nucleons in a ^3S state, and mesons in a P state with a $\cos^2 \theta$ angular distribution. The area under the line spectrum is about 4 times greater than the area under the continuous spectrum. (B) Theoretical spectrum for the final nucleons in a ^1S state, and the meson in a P state with a $\cos^2 \theta$ angular distribution.

Fig. 7 Experimental points and theoretical curves for the differential cross section for the production at 0° of π^+-mesons by 340 Mev protons on protons, as a function of the meson energy. Both theoretical curves are normalized so that the area under each from 65.5 Mev to 76.0 Mev is equal to the area under the experimental points in the same energy interval.

Fig. 8 Neighboring trajectories in a plane perpendicular to the lines of force of a uniform magnetic field.

Fig. 9 Diagram showing the relation between $\Delta\alpha$ and $\Delta\xi$.

Fig. 10 Semi-infinite magnetic field.

Fig. 11 Trajectory leaving the field gap.

Fig. 12 Plan view of trajectory leaving the field gap.

Fig. 13 Thin lens effect of the magnetic field on a meson trajectory.

Fig. 14 Distortion in meson trajectories due to $F_y = \frac{e}{c} v_z \frac{\partial H_z}{\partial x} \Delta Z$.

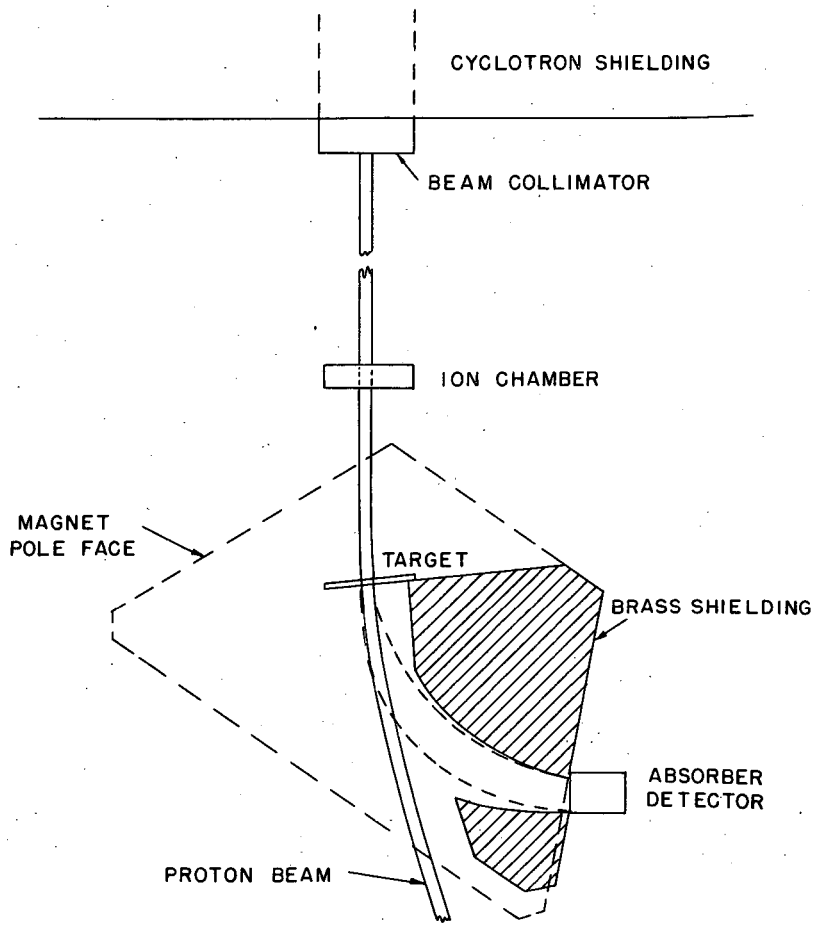
CYCLOTRON SHIELDING
BEAM COLLIMATOR
ION CHAMBER
MAGNET
POLE FACE
TARGET
BRASS SHIELDING
ABSORBER
DETECTOR
PROTON BEAM

FIG. 1

MU 1824

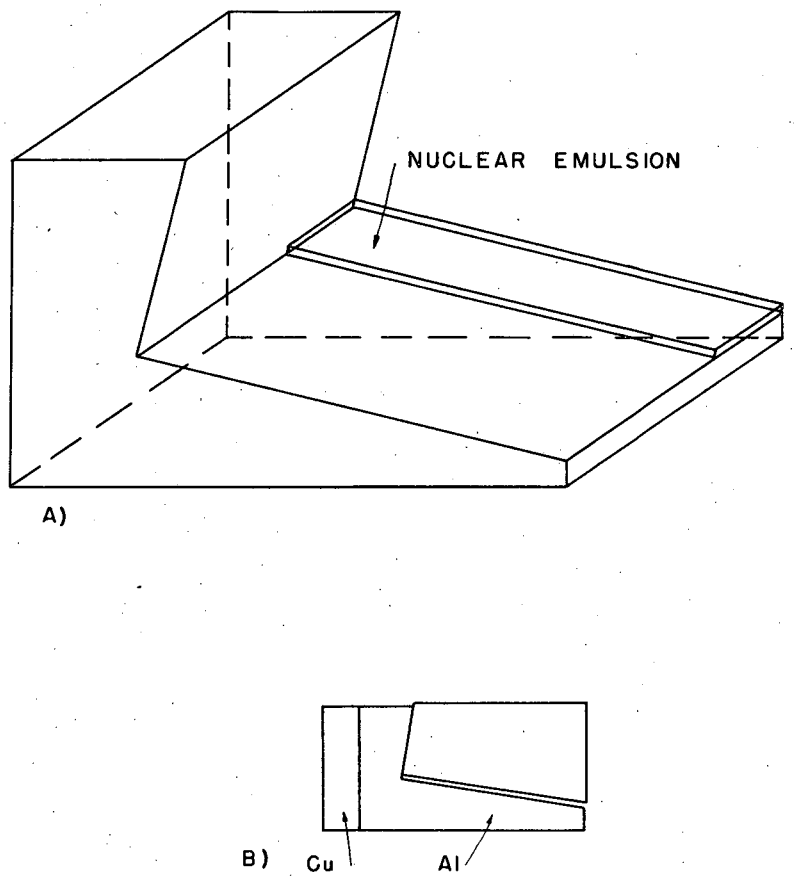

FIG. 2

MU 1825

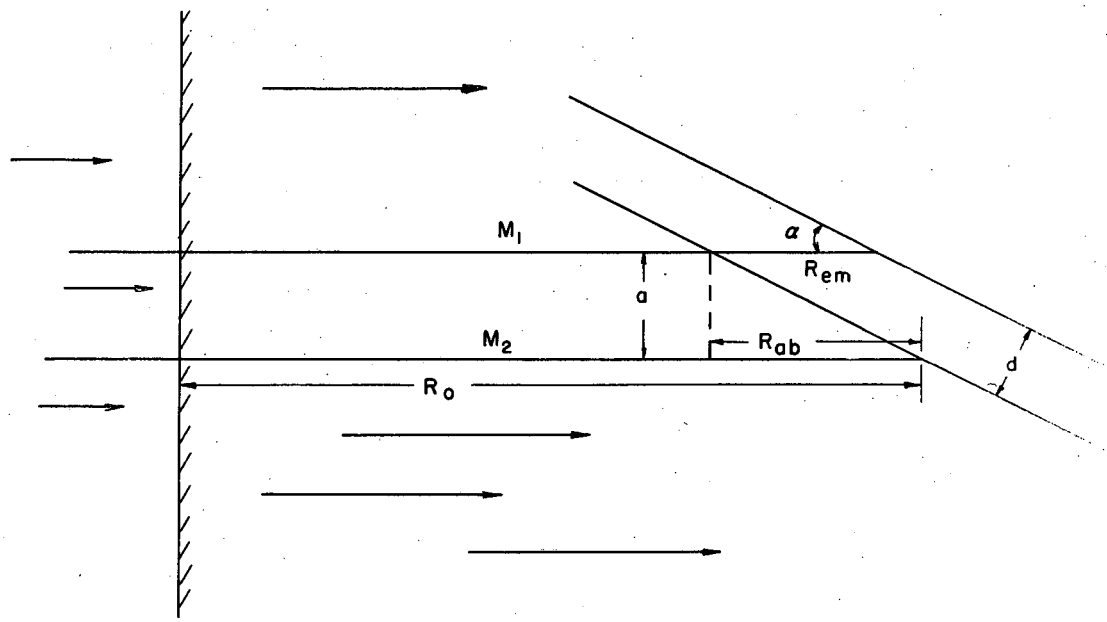

FIG. 3

MU 1826

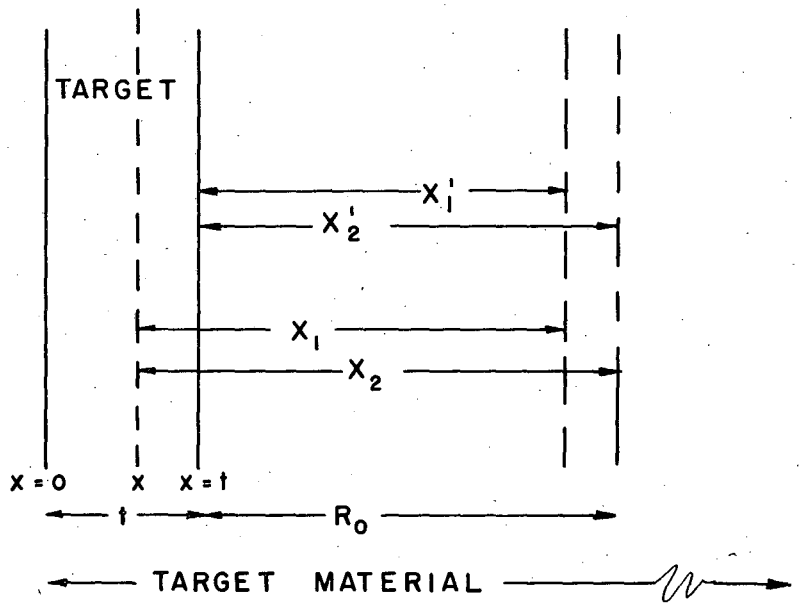

FIG. 4

MU 1827

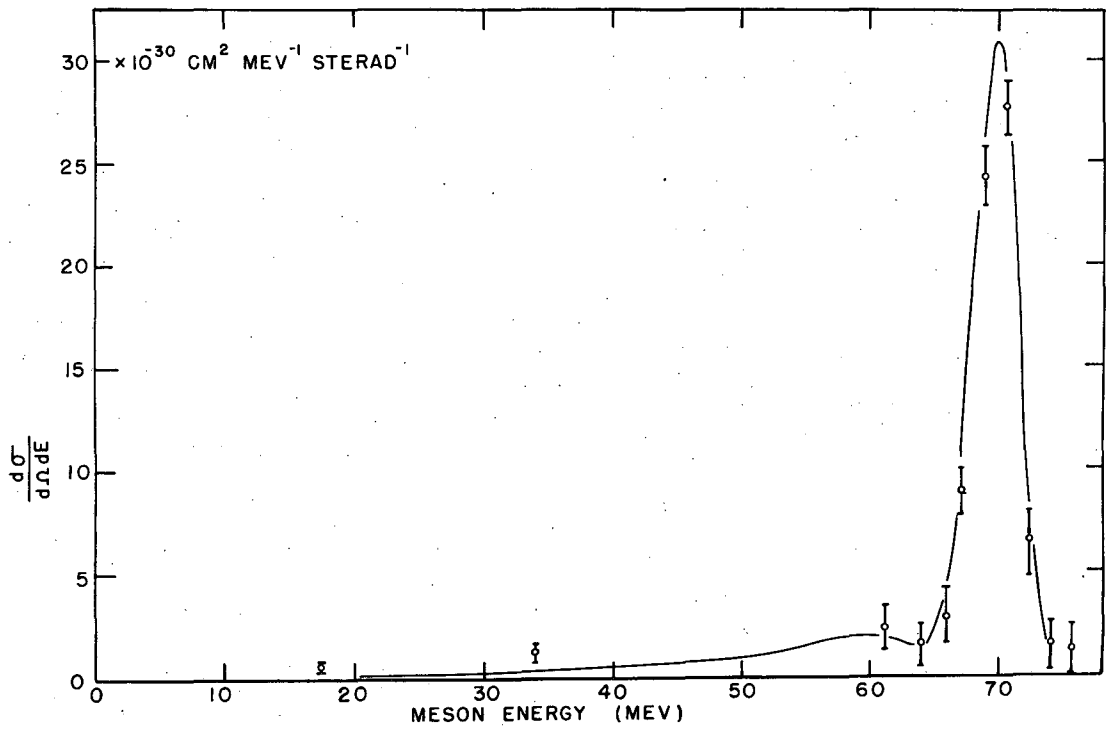
× 10^-30 CM^2 MEV^-1 STERAD^-1
dσ/dΩdE
30
25
20
15
10
5
0
0
10
20
30
40
50
60
70
MESON ENERGY (MEV)

FIG. 5

MU 1828

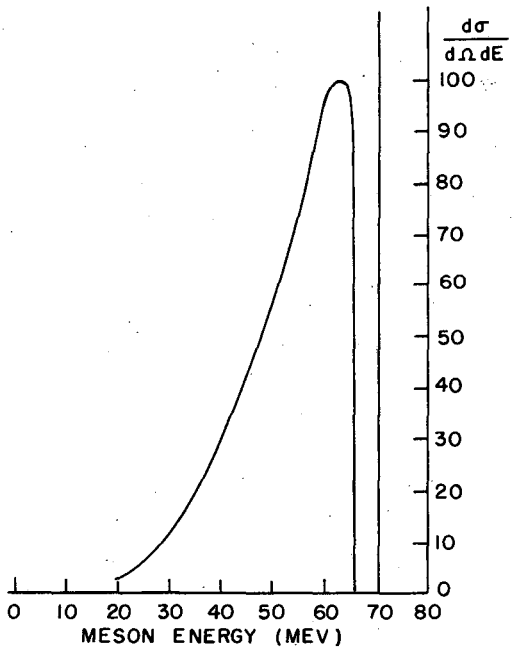

FIG. 6A

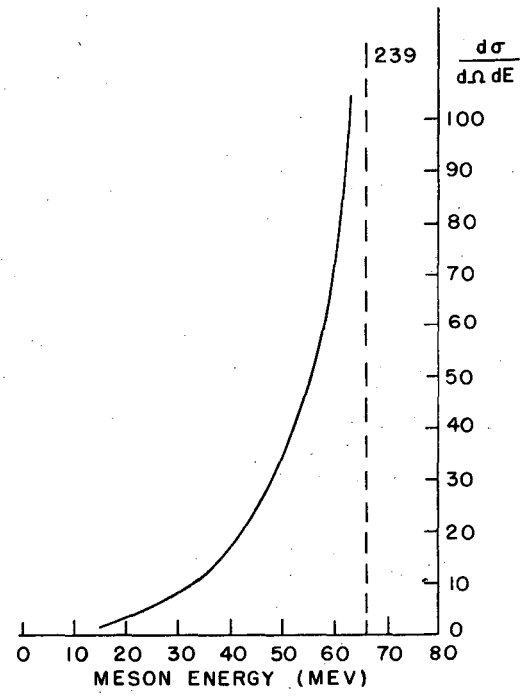

FIG. 6B

MU 1829

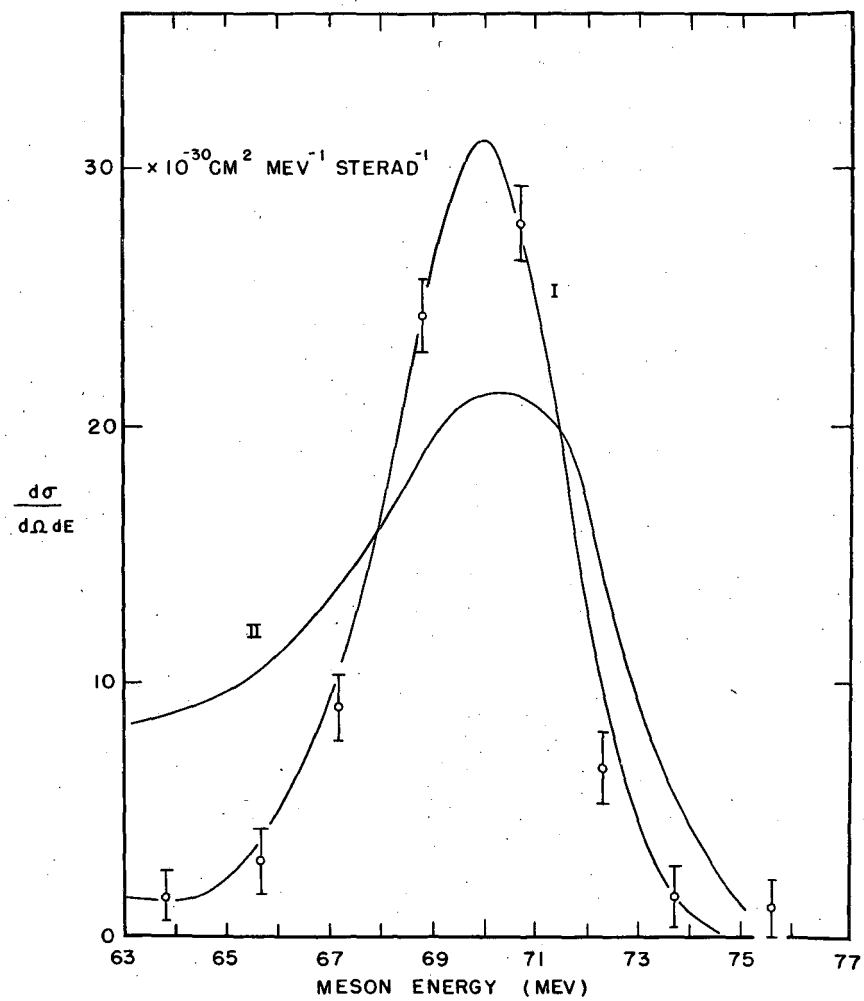
30
20
10
0
× 10^-30 CM^2 MEV^-1 STERAD^-1
dσ / dΩ dE
I
II
63
65
67
69
71
73
75
77
MESON ENERGY (MEV)

FIG. 7

MU 1830

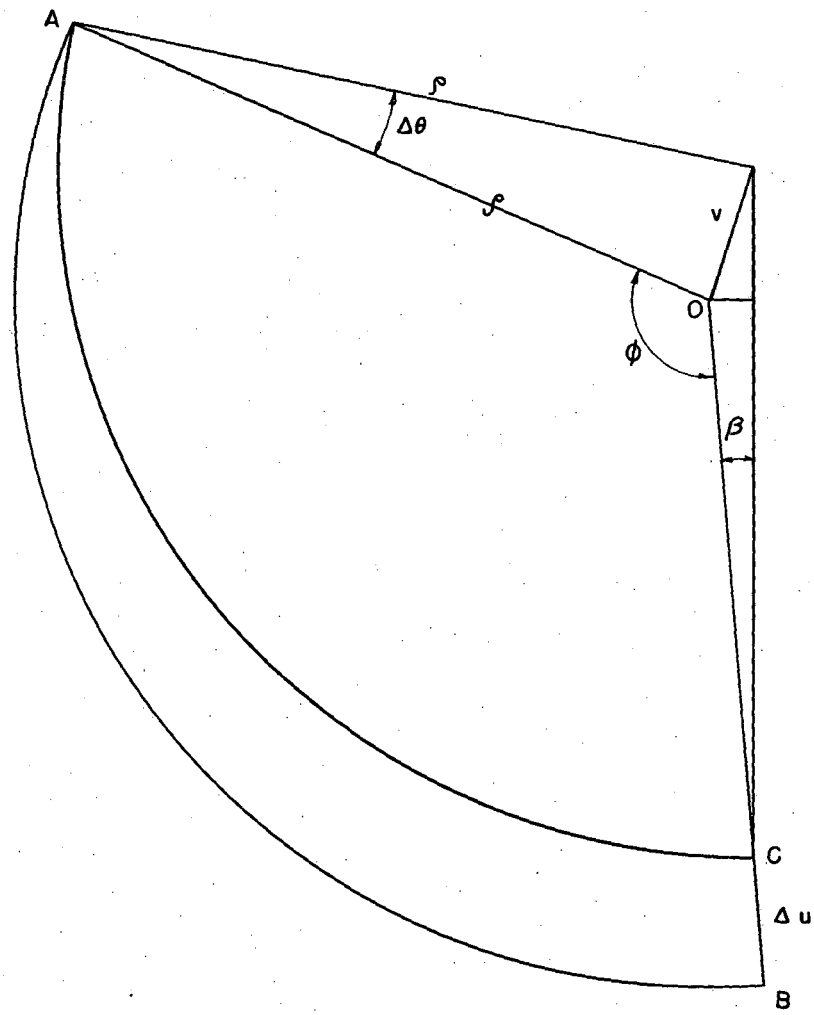

FIG. 8

MU 1831

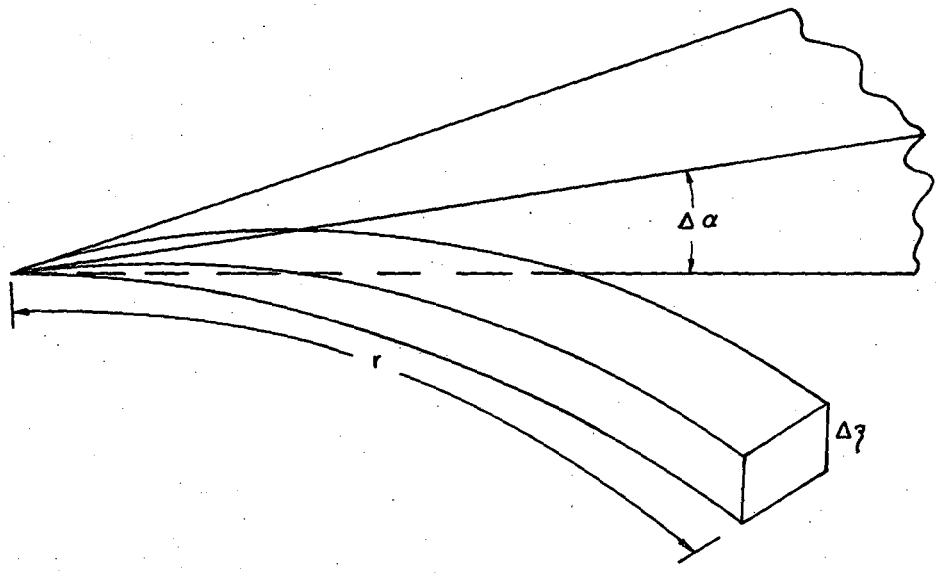

FIG. 9

MU 1832

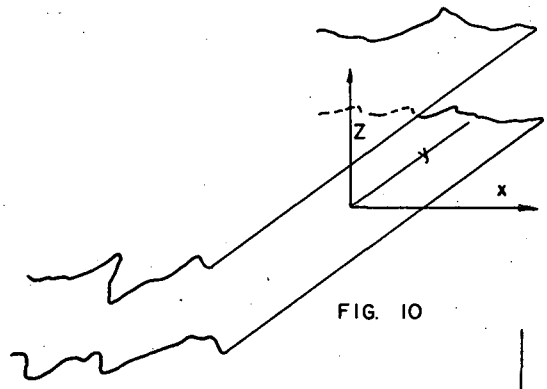

FIG. 10

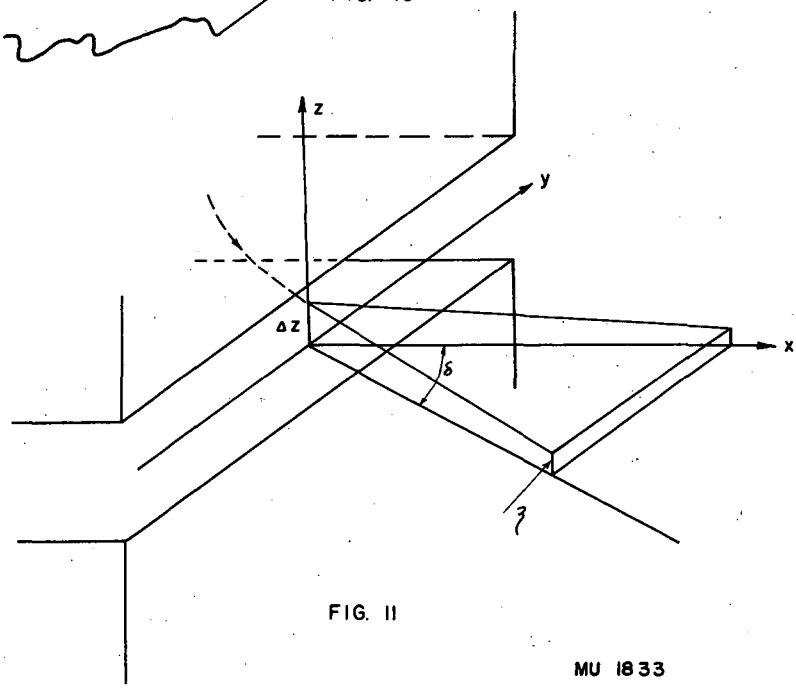

FIG. 11

MU 1833

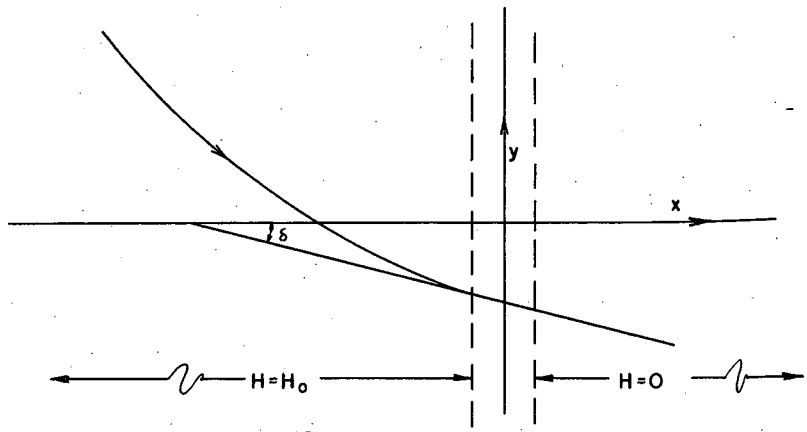

FIG. 12

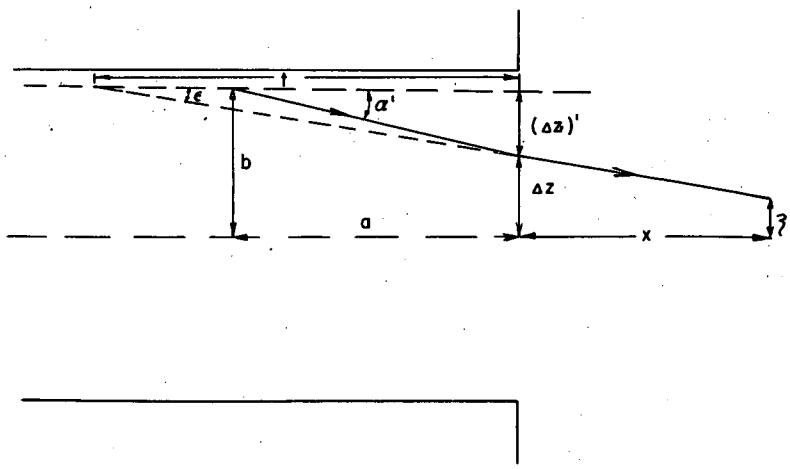

FIG. 13

MU 1834

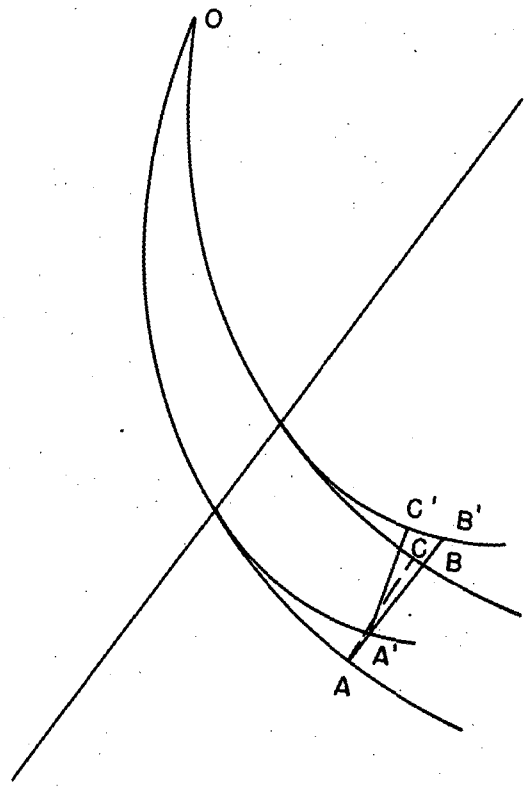

FIG. 14

MU 1835

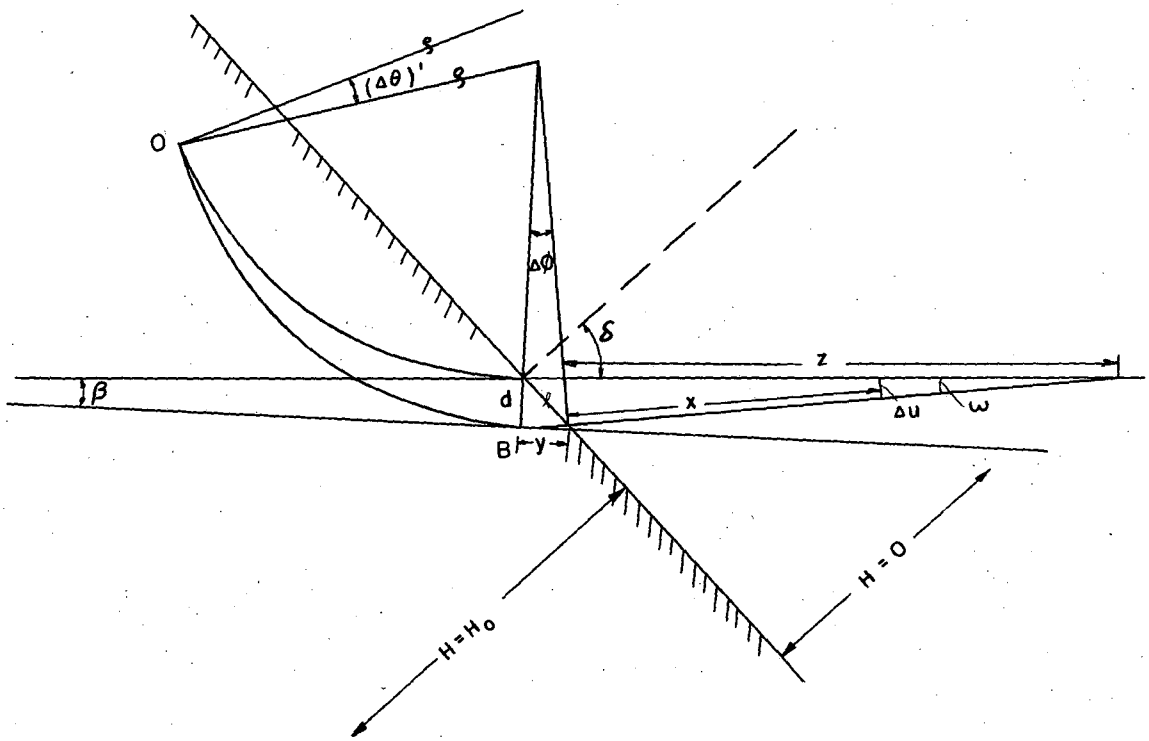

FIG. 15

MU 1836

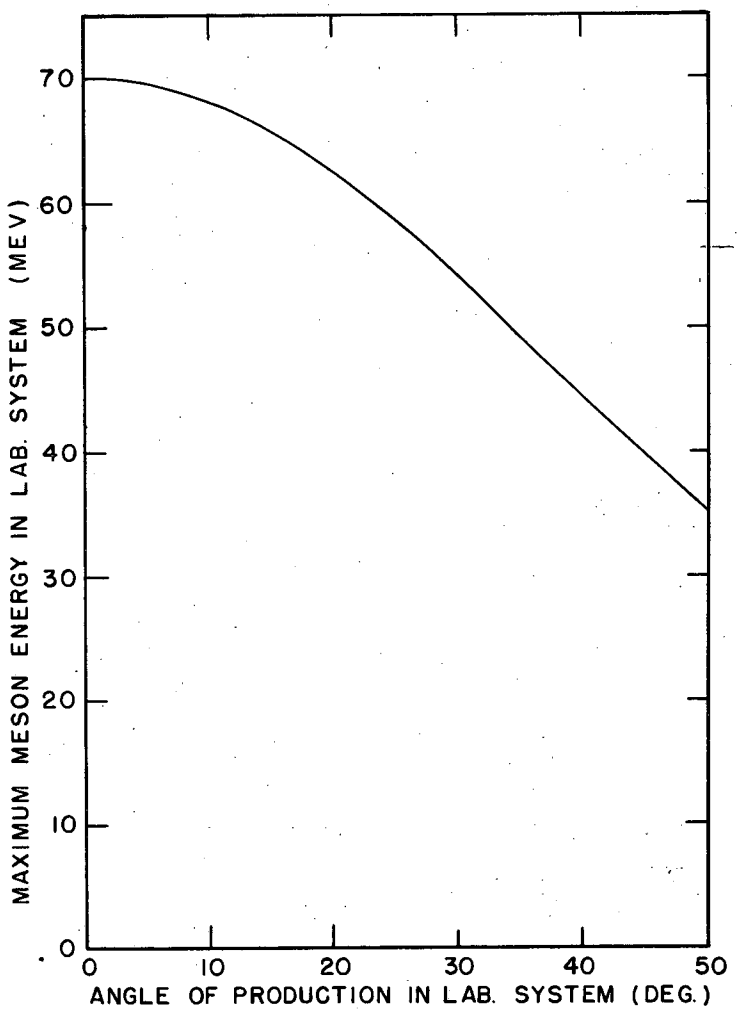

FIG. 16

MU 1837

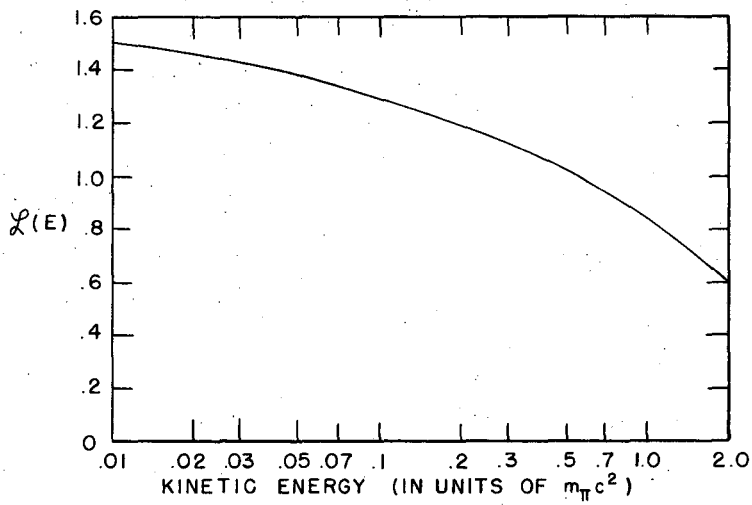

FIG. 17

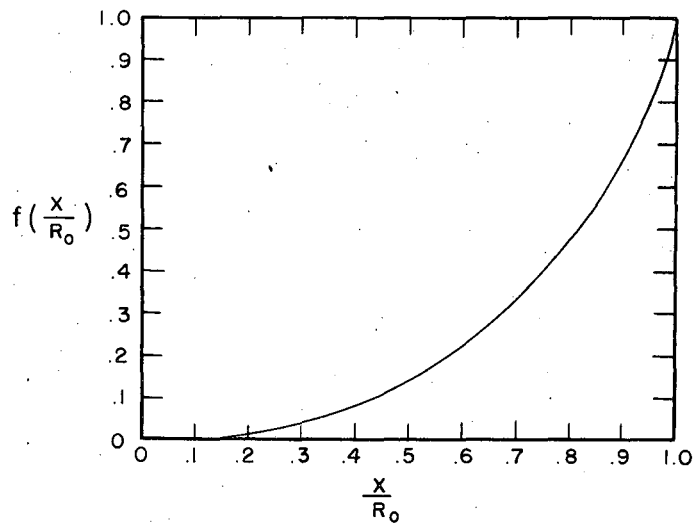

FIG. 18

MU 1838

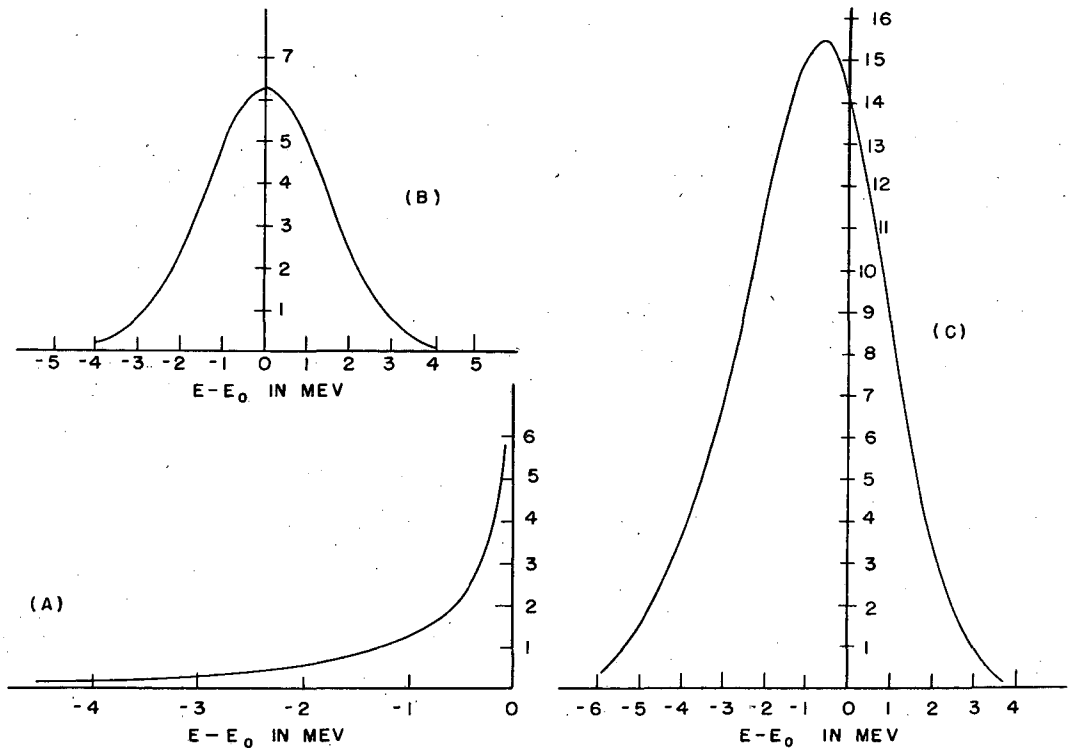

FIG. 19

MU 1839